The Interaction Between Faraday Rotation and System Effects in Synthetic Aperture Radar Measurements of Backscatter and Biomass

Shaun Quegan, *Member, IEEE*, and Mark R. Lomas

***Abstract*—For long-wavelength space-based radars, such as the P-band radar on the recently selected European Space Agency BIOMASS mission, system distortions (crosstalk and channel imbalance), Faraday rotation, and system noise all combine to degrade the measurements. A first-order analysis of these effects on the measurements of the polarimetric scattering matrix is used to derive differentiable expressions for the errors in the polarimetric backscattering coefficients in the presence of Faraday rotation. Both the amplitudes and phases of the distortion terms are shown to be important in determining the errors and their maximum values. Exact simulations confirm the accuracy and predictions of the first-order analysis. Under an assumed power-law relation between σ_{hv} and the biomass, the system distortions and noise are converted into biomass estimation errors, and it is shown that the magnitude of the deviation of the channel imbalance from unity must be 4–5 dB less than the crosstalk, or it will dominate the error in the biomass. For uncalibrated data and midrange values of biomass, the crosstalk must be less than -24 dB if the maximum possible error in the biomass is to be within 20% of its true value. A less stringent condition applies if the amplitudes and phases of the distortion terms are considered random since errors near the maximum possible are very unlikely. For lower values of the biomass, the noise becomes increasingly important because the σ_{hv} signal-to-noise ratio is smaller.**

***Index Terms*—Biomass, calibration, Faraday rotation, long-wavelength radar, polarimetric measurements, system distortion.**

I. Introduction

SEVERAL studies have addressed the interaction between system effects and Faraday rotation in the estimates of geophysical parameters, particularly biomass [1]–[6], but none of them can be considered comprehensive, and a fundamental understanding of these connections is still lacking. However, the selection of the BIOMASS P-band radar mission in May 2013 to be the European Space Agency's Seventh Earth Explorer [7], [8] makes it urgent to gain such insight. This paper aims to achieve this by providing analytic expressions describing how system distortions and noise affect the estimates of the scattering matrix and the covariance matrix of a distributed target in the presence of Faraday rotation. (A companion paper [9] applies a similar approach to quantify the errors in the estimates of the Faraday rotation in the presence of system distortions and noise.) Errors in the covariance matrix are linked to errors in the biomass estimation using a simple biomass inversion scheme.

The basic problem is set out in [1], where it is shown how the measured polarimetric scattering matrix is modified by system distortions, Faraday rotation, and noise when the operating wavelength of the radar becomes sufficiently long. Faraday rotation effects become noticeable at L-band (wavelength $\sim$24 cm) but are an order of magnitude larger at P-band (wavelength $\sim$70 cm) [6]. The calibration of polarimetric measurements when the Faraday rotation can be ignored is well developed [10], [11], as are methods to correct the Faraday rotation when system distortions can be neglected [1], [5], [12], [13]. However, when both are present, correction becomes more difficult since the two effects are coupled in the system of equations connecting the polarimetric measurements to the true scattering matrix.

In Section II, we revisit the calibration problem using the system model in [1], and in Section III, we derive the associated maximum likelihood estimate of the scattering matrix given noisy polarimetric measurements that are affected by Faraday rotation. This provides the starting point for the first-order analysis in Section IV, in which we either assume that the distortion characteristics of the radar (crosstalk and channel imbalance) are imperfectly known in the calibration step or that the system is considered so well engineered that calibration is not performed. From this, we derive differentiable expressions for the errors in the polarimetric backscattering coefficients (see Section V) and conditions under which these are maximized (see Section VI).

In order to test how well the first-order analysis captures the behavior of the system, an exact simulation scheme is also developed, as described in Section VII. This confirms the predictions of the analysis and provides a means to estimate the statistical properties of the estimation errors as the system distortions and noise vary, as illustrated in Section VIII. This fuller depiction of the properties of the measurements is extended to the estimates of the biomass under an idealized power-law relation between the HV backscattering coefficient and the biomass, allowing us to derive conditions on the system distortions and noise in order to keep the relative error in the

Manuscript received March 6, 2014; revised July 23, 2014; accepted December 18, 2014. This work was supported in part by the European Space Agency (ESA) under ESA/European Space Research and Technology Centre (ESTEC) Contract 22849/09/NL/JA/ef, by the U.K. National Environment Research Council through the National Centre for Earth Observation, and by the U.K. Space Agency.

The authors are with the School of Mathematics and Statistics, University of Sheffield, Sheffield S37RH, U.K. (e-mail: s.quegan@sheffield.ac.uk; m.r.lomas@sheffield.ac.uk).

Digital Object Identifier 10.1109/TGRS.2015.2395138

biomass below a given threshold. Here, the simulations are only applied to uncalibrated data; the effectiveness of calibration procedures in reducing the errors in the estimates of the backscatter, the Faraday rotation, and the biomass will form the subject of a separate paper. Conclusions are given in Section IX.

II. System Model

The measured scattering matrix, i.e., $\mathbf{M}$, with Faraday rotation and system errors (channel imbalance, crosstalk, and noise) is given in [1] as

$$\begin{aligned}\mathbf{M} &= \begin{bmatrix} M_{\rm hh} & M_{\rm vh} \\ M_{\rm hv} & M_{\rm vv} \end{bmatrix} \\ &= A(r,\theta)e^{j\varphi}\begin{bmatrix} 1 & \delta_2 \\ \delta_1 & f_1 \end{bmatrix}\begin{bmatrix} \cos\Omega & \sin\Omega \\ -\sin\Omega & \cos\Omega \end{bmatrix}\begin{bmatrix} S_{\rm hh} & S_{\rm vh} \\ S_{\rm hv} & S_{\rm vv} \end{bmatrix} \\ &\quad \times \begin{bmatrix} \cos\Omega & \sin\Omega \\ -\sin\Omega & \cos\Omega \end{bmatrix}\begin{bmatrix} 1 & \delta_3 \\ \delta_4 & f_2 \end{bmatrix} + \begin{bmatrix} N_{\rm hh} & N_{\rm vh} \\ N_{\rm hv} & N_{\rm vv} \end{bmatrix} \quad (1)\end{aligned}$$

where $S_{\rm pq}$, with p and q being either of h or v, are the components of the true scattering matrix, $N_{\rm pq}$ are the additive noise terms, Ω is the Faraday rotation angle, f_1 and f_2 are the channel imbalance terms, and δ_i, $i = 1-4$, are the crosstalk terms. Note that notations $S_{\rm pq}$ and $M_{\rm pq}$ indicate the scattering into channel q from a received signal in channel p, whereas several studies use the opposite (e.g., see [14]). Note also that, for natural targets, we expect that $S_{\rm hv} = S_{\rm vh}$, and we assume this to hold throughout the analysis.

Equation (1) can be written in the following form:

$$\mathbf{M} = A(r,\theta)\, e^{j\theta}\, \mathbf{GFS} + \mathbf{N} \quad (2)$$

where

$$\mathbf{G} = \begin{bmatrix} 1 & \delta_2 & \delta_4 & \delta_2\delta_4 \\ \delta_1 & f_1 & \delta_1\delta_4 & f_1\delta_4 \\ \delta_3 & \delta_2\delta_3 & f_2 & f_2\delta_2 \\ \delta_1\delta_3 & f_1\delta_3 & f_2\delta_1 & f_1 f_2 \end{bmatrix} \quad (3a)$$

$$\mathbf{F} = \begin{bmatrix} c^2 & cs & -cs & -s^2 \\ -cs & c^2 & s^2 & -cs \\ cs & s^2 & c^2 & cs \\ -s^2 & cs & -cs & c^2 \end{bmatrix}. \quad (3b)$$

Here, the measured and true scattering vectors are $\mathbf{M} = [M_{\rm hh}, M_{\rm hv}, M_{\rm vh}, M_{\rm vv}]^T$ and $\mathbf{S} = [S_{\rm hh}, S_{\rm hv}, S_{\rm vh}, S_{\rm vv}]^T$, respectively, $\mathbf{N} = [N_{\rm hh}, N_{\rm hv}, N_{\rm vh}, N_{\rm vv}]^T$ is an additive noise vector, $c = \cos\Omega$, and $s = \sin\Omega$. Since this paper focuses on recovering the polarimetric information, i.e., $\mathbf{S}$, rather than absolute calibration, the scalar term, i.e., $A(r,\theta)e^{j\phi}$, is omitted in the following.

If matrix $\mathbf{G}$ is known, the system distortion can be removed by multiplying (2) by $\mathbf{G}^{-1}$ (which will exist, e.g., see Section IV) to give

$$\mathbf{G^{-1}M} = \mathbf{FS} + \mathbf{G^{-1}N}. \quad (4)$$

This system of equations can be used to estimate Ω from the corrected data, i.e., $\mathbf{G}^{-1}\mathbf{M}$ [1], [5], [12]–[14].

III. Maximum Likelihood Estimate of Scattering Matrix

Since $S_{\rm hv} = S_{\rm vh}$, (4) can be written as

$$M'_i = a_i S_{\rm hh} + b_i S_{\rm hv} + c_i S_{\rm vv} + N'_i, \quad i = 1-4 \quad (5)$$

where

$$\mathbf{M}' = (M'_1,\ M'_2,\ M'_3,\ M'_4)^T = (M'_{\rm hh}, M'_{\rm hv}, M'_{\rm vh}, M'_{\rm vv})^T$$

and $\mathbf{N}' = (N'_1,\ N'_2,\ N'_3,\ N'_4)^T$ are vectors corresponding to the left-hand side (LHS) and the noise term on the right-hand side (RHS) of (4), respectively. The 4×1 coefficient vectors, i.e., $\mathbf{a}$, $\mathbf{b}$, and $\mathbf{c}$, in (5) are given by the elements in the $\mathbf{F}$ matrix, which is calculated using the estimated value of the Faraday rotation, i.e. $\hat{\Omega}$. Thus, from (3b), they take the following form:

$$\begin{aligned}\mathbf{a} &= (\hat{c}^2,\ -\hat{c}\hat{s},\ \hat{c}\hat{s},\ -\hat{s}^2)^T \\ \mathbf{b} &= (0,\ 1,\ 1,\ 0)^T \\ \mathbf{c} &= (-\hat{s}^2,\ -\hat{c}\hat{s},\ \hat{c}\hat{s},\ \hat{c}^2)^T\end{aligned}$$

where $\hat{c} = \cos\ \hat{\Omega}$, and $\hat{s} = \sin\ \hat{\Omega}$. Hence, $(\mathbf{a},\ \mathbf{a}) = (\mathbf{c},\ \mathbf{c}) = 1$, $(\mathbf{b},\ \mathbf{b}) = 2$, and $(\mathbf{b},\ \mathbf{c}) = (\mathbf{c},\ \mathbf{a}) = (\mathbf{a},\ \mathbf{b}) = 0$, where we have used the notation $(\mathbf{x},\ \mathbf{y}) = \sum_{i=1}^{4} x_i y_i^*$. Using these relations, the overdetermined system (5) has a maximum likelihood solution for $\mathbf{S}$ given by (see Appendix 1)

$$\hat{S}_{\rm hh} = \hat{c}^2 M'_{\rm hh} + \hat{c}\hat{s}\ (M'_{\rm vh} - M'_{\rm hv}) - \hat{s}^2 M'_{\rm vv} \quad (6a)$$

$$\hat{S}_{\rm hv} = \frac{M'_{\rm hv} + M'_{\rm vh}}{2} \quad (6b)$$

$$\hat{S}_{\rm vv} = -\hat{s}^2 M'_{\rm hh} + \hat{c}\hat{s}\ (M'_{\rm vh} - M'_{\rm hv}) + \hat{c}^2 M'_{\rm vv}. \quad (6c)$$

Hence, the estimates of $S_{\rm hh}$ and $S_{\rm vv}$ depend on the estimated Faraday rotation angle, but the estimate of $S_{\rm hv}$ does not.

Note that the maximum likelihood solution assumes that the noise terms in (5) are independent zero-mean Gaussian variables all with the same power. If this is true in the original data, it is still very close to being true after correction for system errors, although there is now a weak correlation between some of the noise channels (see Appendix 2).

For biomass recovery, what matters is the effect of errors in the estimate of $\mathbf{G}$ on the covariance matrices of distributed targets [15]–[22], and this forms the focus of the rest of this paper. A companion paper [9] deals with how the errors in the estimate of $\mathbf{G}$ affect the estimates of the Faraday rotation.

IV. First-Order Analysis of System Distortion and Noise Effects on Backscatter Measurements

Equation (4) assumes an exact inverse for $\mathbf{G}$, but in practice, this is unavailable; thus, two approaches are possible.

1) Engineer the radar well enough that the correction for system distortions is unnecessary.
2) Estimate $\mathbf{G}$ to give matrix $\hat{\mathbf{G}}$, and multiply (2) by $\hat{\mathbf{G}}^{-1}$.

$\mathbf{G}$ can be estimated using instrumented calibration sites. This generally requires the effects of Faraday rotation on the

estimate to be accounted for [2]–[4], [23]–[26], but for positions close enough to the magnetic equator, Faraday rotation can be neglected, and methods based on instrumented sites or distributed targets can be used [10], [11], [27].

Whichever approach is taken, (4) will then assume the more realistic form as follows:

$$\hat{\mathbf{M}} = \hat{\mathbf{G}}^{-1}\mathbf{M} = \hat{\mathbf{G}}^{-1}\mathbf{G}\mathbf{F}\mathbf{S} + \hat{\mathbf{G}}^{-1}\mathbf{N} \tag{7}$$

where $\hat{\mathbf{G}}$ is either an estimate of $\mathbf{G}$ or, if no correction is applied, is the identity matrix.

Ignoring second-order terms, $\mathbf{G}$ can be written as

$$\mathbf{G} = \begin{bmatrix} 1 & \delta_2 & \delta_4 & 0 \\ \delta_1 & 1+\varepsilon_1 & 0 & \delta_4 \\ \delta_3 & 0 & 1+\varepsilon_2 & \delta_2 \\ 0 & \delta_3 & \delta_1 & 1+\varepsilon_1+\varepsilon_2 \end{bmatrix} \tag{8}$$

where $\varepsilon_i = f_i - 1$. Note that this assumes that the channel imbalance has been corrected for any significant nonzero mean phase, which is a standard step before level-1A processing, but there might be a small residual unknown phase offset. The first-order inverse of $\mathbf{G}$ is

$$\mathbf{G}^{-1} = \frac{1}{\Delta}\begin{bmatrix} 1+2\varepsilon_1+2\varepsilon_2 & -\delta_2 & -\delta_4 & 0 \\ -\delta_1 & 1+\varepsilon_1+2\varepsilon_2 & 0 & -\delta_4 \\ -\delta_3 & 0 & 1+2\varepsilon_1+\varepsilon_2 & -\delta_2 \\ 0 & -\delta_3 & -\delta_1 & 1+\varepsilon_1+\varepsilon_2 \end{bmatrix} \tag{9}$$

where $\Delta = 1 + 2\varepsilon_1 + 2\varepsilon_2$; this will exist unless $\varepsilon_1 + \varepsilon_2 \approx -1/2$, which would only occur for much larger values of ε_i than would be expected in any well-designed system.

Since the exact inverse of $\mathbf{G}$ is unknown (either because no measurements of the system distortion have been made or because their estimates will inevitably not be perfect), correction for system effects requires the distortion terms in (9) to be replaced by their estimates, i.e., $\hat{\varepsilon}_i$ and $\hat{\delta}_i$, leading to

$$\begin{aligned} \hat{\mathbf{G}}^{-1}\mathbf{G} &= \begin{bmatrix} 1 & \Delta\delta_2 & \Delta\delta_4 & 0 \\ \Delta\delta_1 & 1+\Delta\varepsilon_1 & 0 & \Delta\delta_4 \\ \Delta\delta_3 & 0 & 1+\Delta\varepsilon_2 & \Delta\delta_2 \\ 0 & \Delta\delta_3 & \Delta\delta_1 & 1+\Delta\varepsilon_1+\Delta\varepsilon_2 \end{bmatrix} \\ &= \mathbf{I} + \mathbf{E}_1 + \mathbf{E}_2 \end{aligned} \tag{10}$$

where second-order products have been neglected, $\Delta\delta_i = \delta_i - \hat{\delta}_i$, $\Delta\varepsilon_i = \varepsilon_i - \hat{\varepsilon}_i$, $\mathbf{I}$ is the identity matrix, and error matrices $\mathbf{E}_1$ and $\mathbf{E}_2$ only contain δ and ε terms, respectively, i.e.,

$$\mathbf{E}_1 = \begin{bmatrix} 0 & \Delta\delta_2 & \Delta\delta_4 & 0 \\ \Delta\delta_1 & 0 & 0 & \Delta\delta_4 \\ \Delta\delta_3 & 0 & 0 & \Delta\delta_2 \\ 0 & \Delta\delta_3 & \Delta\delta_1 & 0 \end{bmatrix}$$

$$\mathbf{E}_2 = \begin{bmatrix} 0 & 0 & 0 & 0 \\ 0 & \Delta\varepsilon_1 & 0 & 0 \\ 0 & 0 & \Delta\varepsilon_2 & 0 \\ 0 & 0 & 0 & \Delta\varepsilon_1+\Delta\varepsilon_2 \end{bmatrix}.$$

If no calibration is performed, $\Delta\delta_i$ and $\Delta\varepsilon_i$ should be replaced by δ_i and ε_i, respectively, in these and all subsequent expressions.

Equation (7) can be now written as

$$\hat{\mathbf{M}} = \mathbf{F}\mathbf{S} + (\mathbf{E}_1 + \mathbf{E}_2)\mathbf{F}\mathbf{S} + \hat{\mathbf{G}}^{-1}\,\mathbf{N} \tag{11a}$$

with

$$\mathbf{F}\mathbf{S} = \begin{pmatrix} c^2 S_{\rm hh} - s^2 S_{\rm vv} \\ -cs(S_{\rm hh} + S_{\rm vv}) + S_{\rm hv} \\ cs(S_{\rm hh} + S_{\rm vv}) + S_{\rm hv} \\ -s^2 S_{\rm hh} + c^2 S_{\rm vv} \end{pmatrix} \tag{11b}$$

$$\mathbf{E_1}\mathbf{F}\mathbf{S} = \begin{pmatrix} \Delta\delta_2[FS]_2 + \Delta\delta_4[FS]_3 \\ \Delta\delta_1[FS]_1 + \Delta\delta_4[FS]_4 \\ \Delta\delta_3[FS]_1 + \Delta\delta_2[FS]_4 \\ \Delta\delta_3[FS]_2 + \Delta\delta_1[FS]_3 \end{pmatrix} \tag{11c}$$

$$\mathbf{E_2}\mathbf{F}\mathbf{S} = \begin{pmatrix} 0 \\ \Delta\varepsilon_1[FS]_2 \\ \Delta\varepsilon_2[FS]_3 \\ (\Delta\varepsilon_1 + \Delta\varepsilon_2)\,[FS]_4 \end{pmatrix}. \tag{11d}$$

In (11c) and (11d), $[FS]_i$ denotes the ith component in the 4×1 vector $\mathbf{FS}$.

V. Error in Backscattering Coefficients Due to System Distortion and Noise

Expressions (6) and (11) are now used to provide first-order approximations for the backscattering coefficients. The analysis for $\sigma_{\rm hv}$ differs from that of the copolarized terms because it does not depend on the estimate of the Faraday rotation [see (6)] but is affected by its actual value.

A. Error in Cross-Polarized Backscattering Coefficient $\sigma_{\rm hv}$

The cross-polarized backscattering coefficient, i.e., $\sigma_{\rm hv}$, is crucial in biomass retrieval [15]–[22], and it is therefore critical to know how large its error can be in the presence of system effects. Using (6b) and (11), the first-order approximation for $S_{\rm hv}$ is given by

$$\begin{aligned} \hat{S}_{\rm hv} = S_{\rm hv} + \frac{1}{2}\big\{ & S_{\rm hh}\left(c^2(\Delta\delta_1 + \Delta\delta_3) - s^2(\Delta\delta_2 + \Delta\delta_4)\right) \\ & + S_{\rm vv}\left(c^2(\Delta\delta_2 + \Delta\delta_4) - s^2(\Delta\delta_1 + \Delta\delta_3)\right) \\ & + cs(S_{\rm hh} + S_{\rm vv})(\Delta\varepsilon_2 - \Delta\varepsilon_1) \\ & + S_{\rm hv}(\Delta\varepsilon_1 + \Delta\varepsilon_2) + N'_{\rm hv} + N'_{\rm vh}\big\}. \end{aligned} \tag{12}$$

Notations $N'_{\rm hv}$ and $N'_{\rm vh}$ here refer to the noise terms in (11a) involving the estimate $\hat{\mathbf{G}}^{-1}$, whereas in (5), a similar notation refers to noise terms involving the exact inverse $\mathbf{G}^{-1}$, but this should not cause confusion. In Appendix 3, it is shown that, if the noise is uncorrelated with the signal and between different

channels, the associated estimate of the HV backscattering coefficient, i.e., $\sigma_{\rm hv}$, is

$$\begin{aligned}\hat{\sigma}_{\rm hv} =&\sigma_{\rm hv}|1+\bar{\Sigma}_\varepsilon|^2+\sigma_{\rm hh}|c^2\,\bar{\Sigma}_{13}-s^2\bar{\Sigma}_{24}|^2\\ &+\ \sigma_{\rm vv}|\,c^2\bar{\Sigma}_{24}-s^2\bar{\Sigma}_{13}|^2\\ &+c^2s^2\,(\sigma_{\rm hh}+\sigma_{\rm vv}+2R\cos\theta)|\bar{Y}_{21}|^2\\ &+2{\rm Re}\big\{(c^2\bar{\Sigma}_{13}-s^2\bar{\Sigma}_{24})\left(c^2\bar{\Sigma}^*_{24}-s^2\bar{\Sigma}^*_{13}\right)Re^{j\theta}\big\}\\ &+2cs{\rm Re}\big\{(c^2\,\bar{\Sigma}_{13}-s^2\bar{\Sigma}_{24})(\sigma_{\rm hh}+Re^{j\theta})\,\bar{Y}^*_{21}\\ &\qquad+(c^2\bar{\Sigma}_{24}-s^2\bar{\Sigma}_{13})(\sigma_{\rm vv}+Re^{-j\theta})\bar{Y}^*_{21}\big\}\\ &+2{\rm Re}\left\{S^*_{\rm hv}(1+\bar{\Sigma}^*_\varepsilon)\left[(c^2\,\bar{\Sigma}_{13}-s^2\bar{\Sigma}_{24})S_{\rm hh}\right.\right.\\ &\qquad+(c^2\,\bar{\Sigma}_{24}-s^2\bar{\Sigma}_{13})S_{\rm vv}\\ &\qquad\left.\left.+cs\,(S_{\rm hh}+S_{\rm vv})\,\bar{Y}_{21}\right]\right\}+\sigma'_n/2\end{aligned}\tag{13}$$

where $\sigma_{\rm pq}=\langle|S^2_{\rm pq}|\rangle$, with p and q being either h or v, $\langle S_{\rm hh}S^*_{\rm vv}\rangle=Re^{j\theta}$, $\bar{\Sigma}_{13}=(\Delta\delta_1+\Delta\delta_3)/2$ (the average of the crosstalk from V into H on transmit and the crosstalk from H into V on receive), $\bar{\Sigma}_{24}=(\Delta\delta_2+\Delta\delta_4)/2$ (the average of the crosstalk from H into V on transmit and the crosstalk from V into H on receive), $\bar{\Sigma}_\varepsilon=(\Delta\varepsilon_1+\Delta\varepsilon_2)/2$, $\bar{Y}_{21}=(\Delta\varepsilon_2-\Delta\varepsilon_1)/2$, and we have assumed that the noise terms in the HV and VH channels in (11a) all have the same noise equivalent backscattering coefficient, i.e., σ'_n.

B. Error in Copolarized Backscattering Coefficients $\sigma_{\rm hh}$ and $\sigma_{\rm vv}$

The estimates of the copolarized backscatter [see (6a) and (6c)] depend on the estimated Faraday rotation, but this can be readily taken into account if we assume that the estimation error in the angle is small. Neglecting terms involving second-order products of small quantities, we can then write (see Appendix 4)

$$\begin{aligned}\hat{S}_{\rm hh}\approx&S_{\rm hh}+\frac{S_{\rm hh}}{2}\left\{S(X_{31}-X_{24})+(1-C)\Sigma_\varepsilon\right\}\\ &+\frac{S_{\rm hv}}{2}\left\{(1+C)\Sigma_{24}-(1-C)\Sigma_{31}+SY_{21}\right\}\\ &+\text{noise terms}\end{aligned}\tag{14}$$

$$\begin{aligned}\hat{\sigma}_{\rm hh}\approx&\sigma_{\rm hh}\left\{1+{\rm Re}\left(S(X_{31}-X_{24})+(1-C)\Sigma_\varepsilon\right)\right\}\\ &+{\rm Re}\{S^*_{\rm hh}S_{\rm hv}\left((1+C)\Sigma_{24}-(1-C)\Sigma_{31}+SY_{21}\right)\}\\ &+\sigma'_n\end{aligned}\tag{15}$$

$$\begin{aligned}\hat{S}_{\rm vv}\approx&S_{\rm vv}+\frac{S_{\rm vv}}{2}\left\{S(-X_{31}+X_{24})+(1+C)\Sigma_\varepsilon\right\}\\ &+\frac{S_{\rm hv}}{2}\left\{(1+C)\Sigma_{31}-(1-C)\Sigma_{24}+SY_{21}\right\}\\ &+\text{noise terms}\end{aligned}\tag{16}$$

$$\begin{aligned}\hat{\sigma}_{\rm vv}\approx&\sigma_{\rm vv}\left\{1+{\rm Re}\left(S(-X_{31}+X_{24})+(1+C)\Sigma_\varepsilon\right)\right\}\\ &+{\rm Re}\{S^*_{\rm vv}S_{\rm hv}((1+C)\Sigma_{31}-(1-C)\Sigma_{24}+SY_{21})\}\\ &+\sigma'_n\end{aligned}\tag{17}$$

where $C=\cos(2\Omega)$, $S=\sin(2\Omega)$, $\Sigma_{24}=\Delta\delta_2+\Delta\delta_4$, $\Sigma_{31}=\Delta\delta_3+\Delta\delta_1$, $X_{24}=\Delta\delta_2-\Delta\delta_4$, $X_{31}=\Delta\delta_3-\Delta\delta_1$, $\Sigma_\varepsilon=\Delta\varepsilon_1+\Delta\varepsilon_2$, $Y_{21}=\Delta\varepsilon_2-\Delta\varepsilon_1$, and in (15) and (17), we have again assumed that the noise terms in (11a) all have the same noise equivalent backscattering coefficient, i.e., σ'_n.

VI. Maximizing Errors in Backscattering Coefficients

The expressions derived in Section V are independent of frequency and thus equally apply to P-band and L-band (and higher frequencies). However, when evaluating how large these errors can be, it must be remembered that, at L-band, the Faraday rotation is normally no more than a few degrees (although midlatitude values can be as large as 27° at the solar maximum [28]), whereas at P-band, it is about nine times larger. Hence, although the optimizations over Ω in the following sections allow Ω to take any value in the range from $-\pi$ to π, this range should be constrained depending on the frequency being considered.

A. Maximizing Error in $\sigma_{\rm hv}$

Expression (13) is analytic and is hence easy to evaluate for the given values of the distortion terms, but using it to find the maximum error in $\sigma_{\rm hv}$ as the distortion terms vary is complicated in the general case. However, when the channel imbalance can be neglected and for azimuthally symmetric targets (so that $\langle S_{\rm hh}S^*_{\rm hv}\rangle=\langle S_{\rm vv}S^*_{\rm hv}\rangle=0$ and the term preceding the noise terms in (13) is zero), the following three conditions must be met to give the largest possible error in $\sigma_{\rm hv}$ (see Appendix 3).

1) $\Omega=k\pi/2$; thus, either $\sin^2\Omega=1$, or $\cos^2\Omega=1$.
2) $\arg(\Delta\delta_1)=\arg(\Delta\delta_3)$, and $\arg(\Delta\delta_2)=\arg(\Delta\delta_4)$.
3) All the crosstalk amplitudes should be as large as possible within their constraints.

The largest error occurs when:

- $\arg(\Delta\delta_1)-\arg(\Delta\delta_2)=\theta+2k\pi$ if $\sin^2\Omega=1$, and
- $\arg(\Delta\delta_1)-\arg(\Delta\delta_2)=-\theta+2k\pi$ if $\cos^2\Omega=1$,

where $\theta=\arg\langle S_{\rm hh}S^*_{\rm vv}\rangle$. This largest error has the following modulus:

$$|\hat{\sigma}_{\rm hv}-\sigma_{\rm hv}|=\Delta\delta^2_M(\sigma_{\rm hh}+\sigma_{\rm vv}+2R)+\sigma_n/2\tag{18}$$

where all δ_i have their maximum permitted modulus denoted by $\Delta\delta_M$ (assumed to be the same for all δ_i), $R=|\langle S_{\rm hh}S^*_{\rm vv}\rangle|$, the noise in both the cross-polarized channels in (1) is assumed to have the same noise equivalent σ^0 (NESZ), i.e., σ_n, and we have used Appendix 2 to approximate the modified noise terms by the NESZ of the original data. Note that, for L-band, this maximum error would be only attained when $\Omega=0$, but other values of the Faraday rotation would be relevant at P-band.

B. Maximizing Error in Copolarized Terms

Under reflection symmetry, the second term in (15) is zero, and it is easy to see that the error in $\sigma_{\rm hh}$ due to the crosstalk

will be maximal if X_{31} and X_{24} have phases differing by π and if each has its largest possible real part. If we assume that all the crosstalk terms $\Delta\delta_i$ have the same maximum possible modulus $\Delta\delta_M$, this occurs when $\Delta\delta_i$ are real, with $\Delta\delta_1 = -\Delta\delta_3 = \pm\Delta\delta_M$ and $\Delta\delta_4 = -\Delta\delta_2 = \mp\Delta\delta_M$. Similarly, if both channel imbalance terms $\Delta\varepsilon_i$ have the same maximum possible modulus $\Delta\varepsilon_M$, the error due to the channel imbalance is maximal when $\Delta\varepsilon_1 = \Delta\varepsilon_2 = \pm\Delta\varepsilon_M$, and the maximum error in $\sigma_{\rm hh}$ is then

$$\pm\sigma_{\rm hh}\left(4|S|\Delta\delta_M + 2(1-C)\Delta\varepsilon_M\right).$$

By the same reasoning, the maximum error in $\sigma_{\rm vv}$ is

$$\pm\sigma_{\rm vv}\left(4|S|\Delta\delta_M + 2(1+C)\Delta\varepsilon_M\right).$$

Both errors vary as Ω varies and are maximal when $\tan(2\Omega) = \pm 2\Delta\delta_M/\Delta\varepsilon_M$ (which may not be attainable at L-band, depending on the values of $\Delta\delta_M$ and $\Delta\varepsilon_M$, but could be frequently possible at P-band).

The corresponding maximum error in $\sigma_{\rm hh}$ is

$$\pm 2\sigma_{\rm hh}\left(\Delta\varepsilon_M + \sqrt{4\Delta\delta_M^2 + \Delta\varepsilon_M^2}\right).$$

Replacing $\sigma_{\rm hh}$ by $\sigma_{\rm vv}$ in this expression yields the maximum VV error. However, because the terms involving $X_{31} - X_{24}$ in (15) and (17) have opposite signs and $(1+C)\Sigma_\varepsilon$ and $(1-C)\Sigma_\varepsilon$ have the same sign, both errors cannot be maximized at the same time. Note that these errors can be substantial, e.g., if $\Delta\delta_M = \Delta\varepsilon_M$, the maximum relative error in $\sigma_{\rm hh}$ is given by

$$\frac{\hat{\sigma}_{\rm hh} - \sigma_{\rm hh}}{\sigma_{\rm hh}} = 2(1+\sqrt{5})\,\Delta\delta_M$$

which has a value of 65% if $\Delta\delta_M = 0.1$ (-20 dB) and 20% if $\Delta\delta_M = 0.0316$ (-30 dB).

It should also be noted that the copolarized backscattering coefficients cannot be maximized at the same time as $\sigma_{\rm hv}$ since the former requires the arguments of $\Delta\delta_1$ and $\Delta\delta_3$ (and $\Delta\delta_2$ and $\Delta\delta_4$) to differ by π, whereas the latter requires them to be the same.

VII. Exact Simulations

To test the accuracy of the first-order approximations derived in Section V, we developed a simulator for the measurement process that makes no approximations and directly works from the system model given by (1). In addition, this allows the whole process of biomass estimation from a given data set to be simulated under appropriate assumptions about the relation between the polarimetric measurements and the biomass. In particular, we assume the following:

1) a known relation between the biomass, i.e., B, and the associated covariance matrix, i.e., $C(B)$;
2) a known power-law relation between the biomass and the cross-polarized backscattering coefficient, i.e.,

$$B = A\sigma_{\rm hv}^p \text{ or } \log_{10} B = \log_{10} A + p\times\log_{10}\sigma_{\rm hv}. \quad (19)$$

TABLE I
Covariance Matrix Values for Different Biomass Values

Biomass (t ha^{-1})	σ_{hh} (m^2/m^2)	σ_{vv} (m^2/m^2)	σ_{hv} (m^2/m^2)	R	θ (degs.)
50	0.213	0.250	0.0404	0.086	-54.6
200	0.649	0.274	0.0726	0.150	-96.8
350	1.018	0.281	0.0919	0.172	-139.1

The values used in (19) are $A = 101\,573$ t $\cdot$ ha^{-1} and $p = 2.37521$; these are estimated from the BIOMASS End-to-End Mission Performance Simulator (BEES) [29] and are appropriate for P-band. Together with the values of the covariance terms (see Table I), they are based on airborne measurements over hemiboreal forest stands with biomass ranging from 50 to 270 t $\cdot$ ha^{-1} taken during the 2007 BIOSAR-1 campaign in Sweden; a full description of the field data is given in [20]. Note that, in some calculations, we use biomass values outside the observed range (up to 350 t $\cdot$ ha^{-1}) under the same power law to investigate the sensitivity of errors to the biomass.

Although the biomass can be better estimated by using all polarizations [7], [21], methods to do so rely on regression against a reference data set and would need to be analyzed on an individual basis, almost certainly relying on simulation. In contrast, using a power law (19) only involving $\sigma_{\rm hv}$ as the basis for biomass estimation in this paper allows an analytic treatment and yields insights that would be lost in more complex schemes, as illustrated in Section VIII-A. Furthermore, regression analysis for seven airborne P-band data sets from tropical, temperate, and boreal sites found R^2 values between 0.71 and 0.92 in six out of the seven cases when a linear fit was made to the log–log version of (19), whereas for the seventh case, it was 0.46 (K. Scipal, unpublished manuscript); this yields empirical justification for our simplified approach.

The simulator contains modules that allow the system distortion terms to be estimated from a set of point target measurements by a range of algorithms, e.g., see [4]. These estimates can be then applied to carry out the calibration procedure in (7). However, in the simulations in this paper, no calibration is performed, and errors in the estimates arise purely from uncorrected system distortions and noise.

The simulation involves four steps.

1) *Scene data generation*. For biomass value B, we generate a large set of independent scattering matrix realizations from a zero-mean Gaussian distribution with covariance matrix $C(B)$ using Choleski decomposition. Hence, the data are exactly characterized and can be used to test the validity of the first-order theory without complications introduced by interpixel correlation, point-spread function effects, etc. However, the simulator can readily accept data from other sources, such as real data or the output from BEES [29]. Because terrain effects are not included [30], the simulated data implicitly have reflection symmetry.
2) *Data distortion*. The data are corrupted with system distortions, Faraday rotation, and noise, as in (1). Typically, a set of equally spaced values of Ω covering the range $-\pi < \Omega \leq \pi$ is considered, and for each value

of Ω, many random realizations of the distortion matrix are generated under constraints on the amplitude of the distortion terms but no constraints on the phase.

3) *The estimation of the backscattering coefficients and the biomass*. After estimating Ω at each position using the algorithm in [12], the scattering matrix terms, i.e., S_{pq}, at each pixel are estimated using (6) and are used to estimate $C(B)$. From the estimate of σ_{hv}, B is estimated using (19). Because large windows are used, statistical fluctuations in the estimates of the covariance terms are small, and the perturbations caused by the statistical deviation of the copolarized/cross-polarized correlations from zero are negligible. The errors reported in the following can be therefore seen as irreducible, and a complete error analysis would include the effect of the number of looks on the various estimates.
4) *The derivation of measurement statistics and worst case estimates*. By performing Steps 1–3 for many realizations of the scene and the system distortion matrix, we can derive the histograms of any of the estimated parameters, although of most interest here are σ_{hv} and the biomass. This allows us to assess the accuracy of the first-order theory derived in Sections V and VI, and to visualize the likelihood of worst case errors occurring.

VIII. Testing Predictions From First-Order Analysis

In the top of Fig. 1, we compare the value of $\hat{\sigma}_{\mathrm{hv}}$ derived from (13) with the value from the simulation, as Ω varies, for a single random realization of the distortion matrix and no noise; the calculations are for a biomass of 200 t $\cdot$ ha^{-1} using the covariance values from Table I. The maximum permitted error for both $\Delta\delta_M$ and $\Delta\varepsilon_M$ is taken to be 0.0562 (-25 dB). The approximation is within 0.5% of the simulated value (rising to 1% in the worst case) and reproduces the variation with Ω. This is typical behavior, as indicated by the histogram of the difference between the first-order estimate of σ_{hv} and its exact value from the simulation (see the bottom of Fig. 1). This histogram is derived from 50 000 random values of the crosstalk and the Faraday rotation, with the crosstalk amplitude constrained not to exceed 0.0562 (-25 dB). The error is mean zero and always less than 4×10^{-4} m$^2 \cdot$ m^{-2}, which confirms the ability of the first-order approximation to represent system effects accurately.

The values for the maximum (18) and the corresponding relative error, i.e., $(\hat{\sigma}_{\mathrm{hv}} - \sigma_{\mathrm{hv}})/\sigma_{\mathrm{hv}}$, when $\Delta\delta_M = 0.0562$ and the channel imbalance and the noise are neglected are given in the second and third columns in Table II for different biomass values using the covariance values from Table I. The relative error in σ_{hv} ranges from 5% to 6%. However, the channel imbalance can cause the maximum errors to increase significantly, as can be seen from the leading term on the RHS of (13). If considered in isolation, to first order a channel imbalance $\bar{\Sigma}_\varepsilon$ yields an error in σ_{hv} of order $2\bar{\Sigma}_\varepsilon$, e.g., a channel imbalance of 0.0562 can cause an error of 12% in σ_{hv}. Comparing this value with the errors due to the crosstalk in Table II indicates that, if the crosstalk and the channel imbalance are similar in magnitude, the latter will dominate the error in σ_{hv}. The essential reason for this is that, in (13), there is a term multiplying σ_{hv} that is linear in the channel imbalance, whereas all other terms involve the quadratic products of the distortion terms. [Although if the copolarized/cross-polarized Hermitian products are retained, other terms that are linear in the distortion arise, as shown in (13)]. Hence, although the true copolarized powers are larger, the errors involving them will be dominated by this linear term unless the channel imbalance is much smaller than the crosstalk.

The fourth and fifth columns in Table II give the maximum and relative maximum errors derived from the simulation under

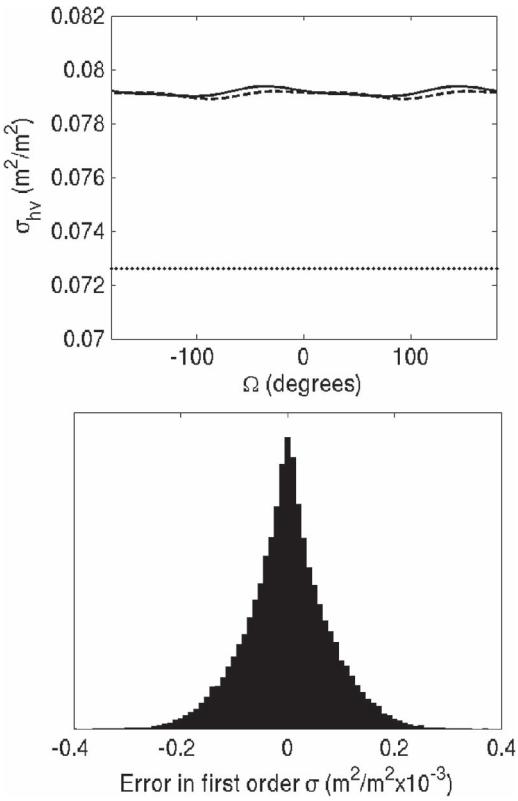

Fig. 1. (Top) First-order approximation (dashed curve) and simulated value (solid curve) of σ_{hv} as a function of Ω for a single random realization of the system distortion with no noise. The true value of σ_{hv}, corresponding to a biomass of 200 t $\cdot$ ha^{-1}, is indicated by the horizontal dotted line. The amplitudes of distortion terms δ_i and ε_i were constrained not to exceed 0.0562 (-25 dB). (Bottom) Error in the first-order estimate of σ_{hv} derived from (13) compared with its value from the simulation for 50 000 random values of the crosstalk amplitude and the Faraday rotation, with a maximum permitted amplitude of crosstalk $= 0.0562$.

TABLE II
Maximum and Relative Errors in the HV Backscattering Coefficient for Different Biomass Densities Derived From (18) and by Simulation, Assuming That the Channel Imbalance and the Noise Are Negligible, and the Maximum Permitted Error in the Crosstalk Is 0.0562 (-25 dB)

Biomass (t ha^{-1})	$\hat{\sigma}_{hv}-\sigma_{hv}$	$\frac{\hat{\sigma}_{hv}-\sigma_{hv}}{\sigma_{hv}}$	$\sigma_{hv}^{sim}-\sigma_{hv}$	$\frac{\sigma_{hv}^{sim}-\sigma_{hv}}{\sigma_{hv}}$
50	0.00201	0.0497	0.00233	0.0577
200	0.00387	0.0533	0.00443	0.0610
350	0.00520	0.0566	0.00580	0.0632

the same conditions. These are larger, indicating that the first-order approximation leads to slight underestimates of the worst possible error.

The worst case errors in $\sigma_{\rm hv}$ occur for particular combinations of the Faraday rotation and the magnitudes and phases of the distortion terms. To investigate how likely these are, the errors were calculated for 50 000 random realizations of the crosstalk and the Faraday rotation, with no channel imbalance and noise, for a biomass of 200 t $\cdot$ ha^{-1}, leading to the histograms of errors in $\sigma_{\rm hv}$ in Fig. 2. In Fig. 2(a), the crosstalk amplitude is random and constrained not to exceed 0.0562, whereas in Fig. 2(b), it is fixed at 0.0562. In both cases, the maximum error predicted by (18) is 0.00387, which is indicated by the vertical dotted lines, whereas the maximum from the simulation is 0.00443 (dashed lines). The maximum error in $\sigma_{\rm hv}$ occurs far out in the tail of the distribution, and even when all the crosstalk amplitudes are set to their maximum possible values, the proportion of phase variations giving large errors is small.

This is made more precise by the cumulative density functions corresponding to Fig. 2(a) and (b) shown in Fig. 2(c) (solid and dashed lines, respectively). In the first case, there is only a 1% probability that the error exceeds 1.5×10^{-3} m$^2 \cdot$ m^{-2}, whereas the corresponding value in the second case is 3.3×10^{-3} m$^2 \cdot$ m^{-2}.

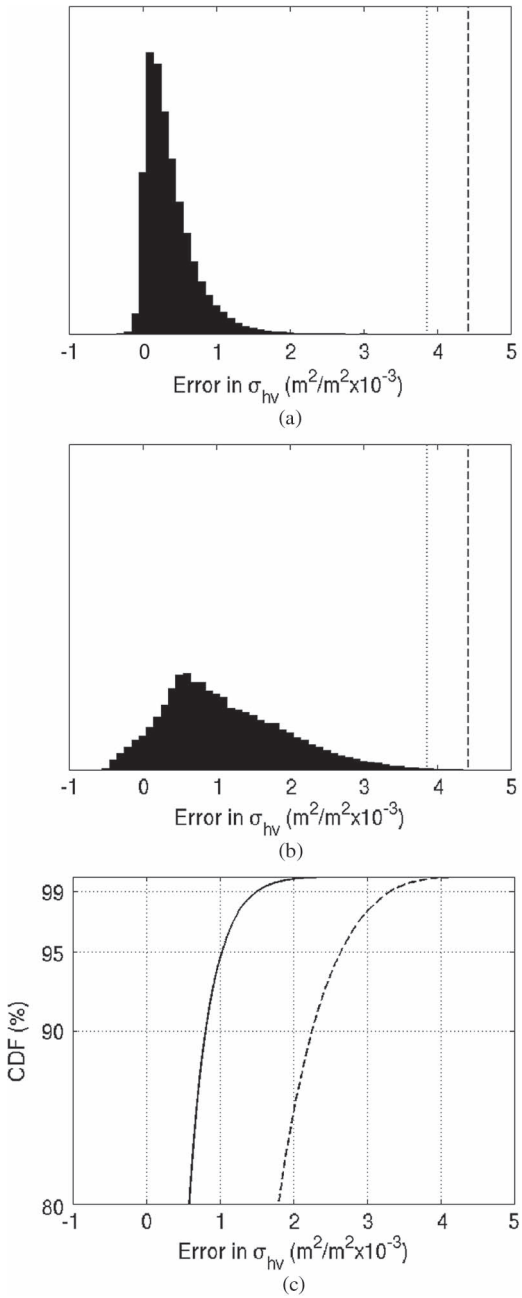

Fig. 2. Histograms of the error in $\sigma_{\rm hv}$ for a forest with a biomass of 200 t $\cdot$ ha^{-1}, which are derived from 50 000 random values of the crosstalk and the Faraday rotation, neglecting the channel imbalance and the noise, with (a) the maximum permitted amplitude of the crosstalk $= 0.0562$ and (b) the crosstalk amplitude fixed at 0.0562. The maximum error predicted by (18) is 0.00387 and is indicated by the vertical dotted lines. The true maximum error is 0.00443 (dashed lines). (c) Cumulative distribution functions corresponding to (a) (solid line) and (b) (dashed line).

A. Maximum Error in Estimated Biomass

The errors in $\sigma_{\rm hv}$ due to the system distortion, i.e., $\Delta\sigma_{\rm hv}$, and the noise, i.e., $\sigma_n/2$, [the first and second terms on the RHS of (18)) can be readily converted to a biomass error using (19) since the estimated biomass, i.e., $\hat{B}$, can be written as

$$\begin{aligned}\hat{B} &= A(\sigma_{\rm hv} + \Delta\sigma_{\rm hv} + \sigma_n/2)^p \\ &= A\sigma_{\rm hv}^p \left(1 + \frac{\Delta\sigma_{\rm hv}}{\sigma_{\rm hv}} + \frac{\sigma_n}{2\sigma_{\rm hv}}\right)^p \\ &\approx B\left(1 + p\left\{\frac{\Delta\sigma_{\rm hv}}{\sigma_{\rm hv}} + \frac{\sigma_n}{2\sigma_{\rm hv}}\right\}\right) \qquad (20)\end{aligned}$$

where the approximation is valid if $\Delta\sigma_{\rm hv} \ll \sigma_{\rm hv}$ and $\sigma_n \ll \sigma_{\rm hv}$. Hence, the relative errors from the system distortion and the noise are approximately additive and given by $p\Delta\sigma_{\rm hv}/\sigma_{\rm hv}$ and $p\sigma_n/(2\sigma_{\rm hv})$, respectively. This provides an easy way to estimate the relative error and to quantify the constraints on the total calibration error and noise to keep this error within desired bounds. Note that (20) does not take into account any errors in the constant A or exponent p; since these would normally be estimated from the reference data, a full error analysis would have to include the associated uncertainties (e.g., in [21], the estimates of p had uncertainties of about 8%).

Table III gives the worst case estimates of the biomass for forests with biomass densities of 200 and 350 t $\cdot$ ha^{-1}, which are derived from both the numerical optimization and the first-order analysis, where both use the exact expression in (20). The maximum permitted crosstalk amplitude is 0.0562, and the channel imbalance and the system noise are neglected. As predicted, all the crosstalks take their maximum amplitude, $\arg(\delta_1) = \arg(\delta_3), \arg(\delta_2) = \arg(\delta_4)$, and the same maximum error occurs when Ω takes any multiple of $\pi/2$ as long as the appropriate phase relationships hold. For a biomass of 200 t $\cdot$ ha^{-1}, $\theta = -96.8^\circ$ (see Table I); the first-order analysis then predicts that $\arg(\delta_1) - \arg(\delta_2) = 96.8^\circ$ when $\Omega = 0^\circ$ or 180° (the value from the optimization is 96.2°) and that $\arg(\delta_1) - \arg(\delta_2) = -96.8^\circ$ when $\Omega = \pm 90^\circ$ (the optimized

TABLE III
MAXIMUM BIOMASS ERRORS FOR FORESTS OF 200 AND 350 t · ha^{-1}, AND THE CROSSTALK PHASE VALUES UNDER WHICH THEY OCCUR, WHICH ARE DERIVED FROM NUMERICAL OPTIMIZATION WHEN CHANNEL IMBALANCE AND SYSTEM NOISE ARE NEGLECTED. THE FIRST-ORDER PREDICTIONS OF THE MAXIMUM BIOMASS ERROR ARE ALSO GIVEN. THE MAXIMUM PERMITTED AMPLITUDE OF THE CROSSTALK IS 0.0562

	200 t ha^{-1}		350 t ha^{-1}	
Ω (degrees)	0, 180	-90, 90	0, 180	-90, 90
arg(δ_1), arg(δ_3) (degrees)	-147.7	-63.9	62.1	108.4
arg(δ_2), arg(δ_4) (degrees)	116.1	32.3	-73.3	-114.8
Biomass (t ha^{-1}) (optimisation)	231	231	405	405
Biomass (t ha^{-1}) (1st order est.)	227	227	399	399

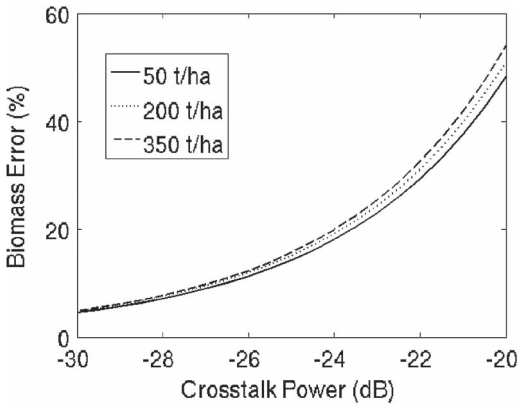

Fig. 3. Maximum percentage error in the retrieved biomass for three values of the biomass as the crosstalk magnitude varies when the channel imbalance and the noise are neglected.

value is $-96.2°$). The corresponding values for a biomass of 350 t · ha^{-1} are $\arg(\delta_1) - \arg(\delta_2) = 139.1°$ when $\Omega = 0°$ or 180° and $\arg(\delta_1) - \arg(\delta_2) = -139.1°$ when $\Omega = \pm 90°$ (the optimized values are 135.4° and $-135.4°$, respectively). Hence, the theory agrees well with the observations, particularly for the biomass of 200 t · ha^{-1}.

Note that the errors in Table III lie within the 20% target for BIOMASS [7], although these are maximum possible errors and hence very unlikely, as discussed earlier. In fact, when the channel imbalance and the noise are neglected, the crosstalk amplitude needs to exceed -24 dB for the 20% threshold to be breached. This is demonstrated in Fig. 3, which also indicates that higher values of the biomass require slightly lower values of $\Delta\delta_M$ to keep the percentage error below a given value. For example, a maximum possible error of 20% in the biomass requires $\Delta\delta_M < -23.6$ dB for a biomass of 50 t · ha^{-1}, but this reduces to -24.0 dB for a biomass of 350 t · ha^{-1}.

It should be remembered that the maximum error occurs under specific conditions on the amplitude and phase of the crosstalk terms. To assess the likelihood of these occurring, histograms of the biomass error for a biomass of 200 t · ha^{-1} were derived from 50 000 random realizations of the crosstalk with no channel imbalance [see the top of Fig. 4(a)] and the channel imbalance with no crosstalk [see the bottom of Fig. 4(a)]. The maximum amplitude of the distortion terms is taken to be 0.0316, 0.0562, or 0.1 (-30, -25, or -20 dB, respectively), and their phases and that of Ω are uniformly distributed between $-\pi$ and π. The vertical bars indicate the maximum observed errors, which are also given in Table IV. Fig. 4(b) is similar, but here, the distortion terms are fixed at their maximum values and only the phases are randomized. As predicted, the maximum error in $\sigma_{\rm hv}$ occurs when all the distortion terms adopt their maximum values; thus, the maximum values are the same in Fig. 4(a) and (b). In addition, as predicted, the maximum error from the channel imbalance is larger than that from the crosstalk if their magnitudes are similar.

If the channel imbalance is neglected, the maximum error in the biomass is less than 20%, even if the crosstalk is as large as -24 dB, but exceeds 20% if the channel imbalance has a value of -28 dB with no crosstalk. However, as shown in Fig. 4(a), the maximum error occurs very far out in the tail of the distribution when the amplitude of the distortions is randomly distributed (up to some maximum value) since it requires all the distortion terms to take their largest permitted amplitudes and particular relations to hold among their phases. If all the distortion terms are fixed at their maximum amplitudes, then the maximum error occurs more frequently [see Fig. 4(b)] since it will arise from many different phase arrangements as long as they obey the conditions preceding (18).

The maximum percentage biomass error when both crosstalk and channel imbalance are present is shown as a contour plot in Fig. 5. It can be seen that, to keep the error below 20%, the channel imbalance and the crosstalk must not exceed -28 and -24 dB, respectively. For crosstalks of -30 and -25 dB, the corresponding limits on the channel imbalance to keep the relative error below 20% are -31 and -41 dB, respectively, whereas if the crosstalk reaches -20 dB, the maximum error always lies well above 40%. Again, it should be noted that these are worst possible cases and are hence of low probability.

The biomass percentage error due to the noise alone is shown in Fig. 6 for three levels of the biomass. The noise is particularly damaging for lower biomass forests because of their lower values of $\sigma_{\rm hv}$. Keeping the error below 20% requires the NESZ to be less than -22 dB for a biomass of 50 t · ha^{-1}, which relaxes to NESZ < -18.6 dB for a biomass of 350 t · ha^{-1}.

IX. CONCLUSION

This paper has provided first-order approximations to the errors in the polarimetric backscattering coefficients caused by system distortions and noise in the presence of Faraday rotation, thus giving a clear insight into the factors controlling these errors. The approximations are differentiable and can be used to derive conditions on the amplitudes and phases of the crosstalk and channel imbalance terms that yield the greatest possible errors in the backscattering coefficients given the constraints on the amplitudes. To first order, we found the following to be true.

- The error in $\sigma_{\rm hv}$ depends on the true value of $\sigma_{\rm hv}$ only through the channel imbalance but has contributions from $\sigma_{\rm hh}$ and $\sigma_{\rm vv}$ arising from both the channel imbalance and the crosstalk.

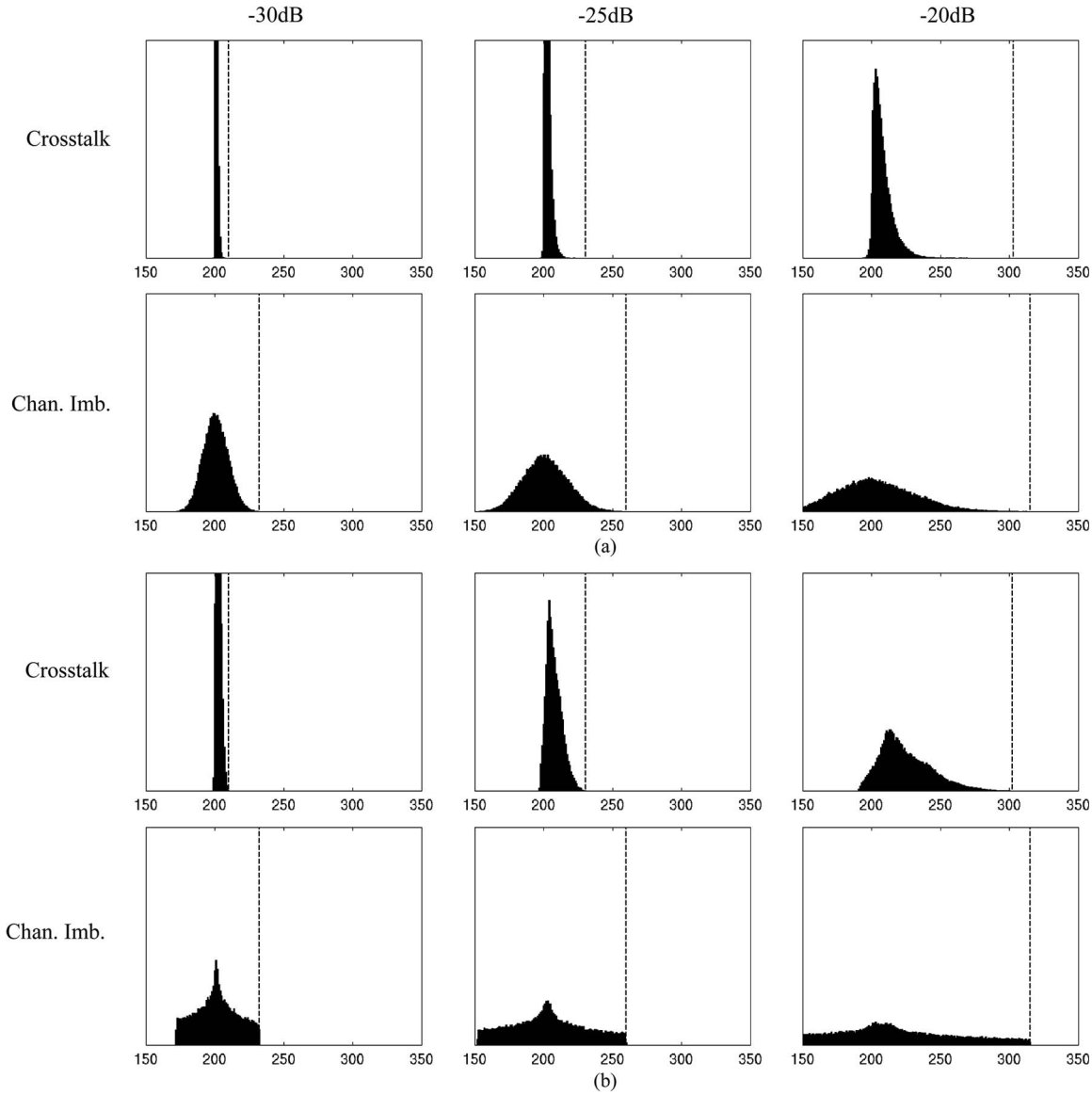

Fig. 4. (a) Histograms of the retrieved biomass for a biomass of 200 t · ha^{-1} for 50 000 random samples of (top row) crosstalk with no channel imbalance and (bottom row) channel imbalance with no crosstalk, together with Faraday rotation. In each sample, the amplitude of δ or ε is uniformly generated in the range of (left to right) 0–0.0316, 0–0.0562, or 0–0.1, i.e., -30, -25, and -20 dB, respectively, and the phase, together with that of Ω, is uniformly distributed between $-\pi$ and π. The vertical lines mark the maximum observed biomass. (b) Same as (a), except that, in each sample, the amplitude of δ or ε is set to the fixed value 0.0316, 0.0562, or 0.1.

TABLE IV
MAXIMUM BIOMASS ERRORS PRODUCED BY THE SIMULATION FOR A FOREST WITH A BIOMASS OF 200 t · ha^{-1} WHEN ONLY THE CROSSTALK OR ONLY THE CHANNEL IMBALANCE IS CONSIDERED FOR THREE LEVELS OF THE MAXIMUM DISTORTION AMPLITUDE

Amplitude of distortions	Max. biomass error (t ha^{-1}); cross-talk only	Max. biomass error (t ha^{-1}); channel imbalance only
0.0316	9.7	31.9
0.0562	30.2	59.5
0.1000	102.7	114.8

- The error in $\sigma_{\rm hh}$ depends on $\sigma_{\rm hh}$ and $\langle S^*_{\rm hh} S_{\rm hv}\rangle$ (but not on $\sigma_{\rm vv}$), both of which have coefficients that are linear in the distortion terms; equivalent remarks apply to the error in $\sigma_{\rm vv}$.

In both cases, the system noise makes an independent additive contribution to the error. The analysis is applicable to any radar frequency, but the calculation of the maximum possible errors must take into account that the range of possible Faraday rotation angles depends on the frequency.

Exact simulations confirm the predictions of the first-order analysis and can be used to investigate the complete process, from the measured data to the estimates of the biomass under any given relationship between the biomass and the backscattering coefficients; they can be also used to empirically derive the statistical properties of the various estimates. The simplified analysis here assumes a known power-law relationship between the biomass and $\sigma_{\rm hv}$, and it is most appropriate for P-band data; however, the simulation approach can be readily used to investigate effects such as uncertainty in the power-law exponent, other forms of the relationship between the biomass and $\sigma_{\rm hv}$, more complex relationships between the biomass and the full set of backscattering coefficients, etc.

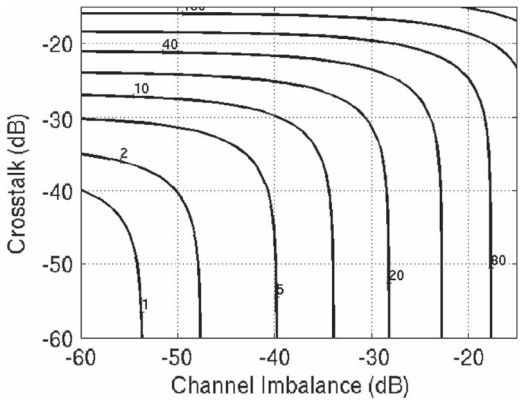

Fig. 5. Contour plot of the maximum percentage error in the biomass for a forest of 200 t · ha^{-1} as the crosstalk and channel imbalance amplitudes vary. Contours are labeled with percentage error.

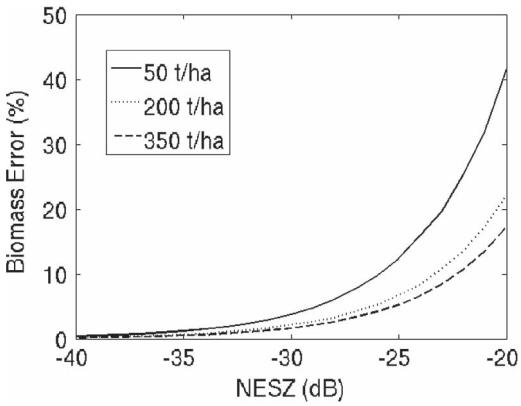

Fig. 6. Percentage error in the retrieved biomass for three values of the biomass solely due to the noise without system distortions.

The following were demonstrated.

1) The deviation of the channel imbalance from unity causes greater errors in $\sigma_{\rm hv}$ than the crosstalk if their amplitudes are comparable, and to yield similar errors, it must be kept to levels around 4–5 dB less than the crosstalk. In contrast, the maximum error in the estimate of the Faraday rotation is insensitive to the channel imbalance and is almost entirely controlled by the crosstalk amplitude [9].
2) The phases of the distortion terms have significant effects on the size of the errors in the backscattering coefficients and the biomass, and the worst possible errors occur for particular phase relationships between the distortion terms.
3) If the phase and amplitude errors are considered random, errors near the largest possible value are very unlikely to occur, and weaker conditions on the crosstalk and channel imbalance amplitudes are acceptable to meet the target accuracy on the backscattering coefficients and the biomass.

It is important to note that the aim of this paper has been to provide insight into how system distortions and Faraday rotation affect the estimates of the backscattering coefficients and the biomass, and it therefore adopts simplifications that would need to be relaxed for a complete error analysis in a more general situation. Issues to be considered in such an analysis include the following.

1) More complete algorithms to retrieve the biomass use the full polarimetric covariance matrix, not just the HV backscattering coefficient [7], [21].
2) Many of the world's forests are in hilly areas; this gives rise to distortion of the covariance matrix and nonzero correlation between the copolarized and cross-polarized channels, and correction methods exploit the full covariance matrix [30].
3) The algebraic analysis does not account for statistical fluctuations in the estimates of the covariance terms, and the simulations use windows that are so large that these can be neglected. The effect of the number of looks on the errors therefore has not been studied in this paper.

Although it may be possible to extend the algebraic analysis to partly cover these more general conditions, it is likely that their investigation would have to lean heavily on simulation.

Appendix 1
Maximum Likelihood Estimate of S

Equation (4) can be written as

$$M_i' = a_i S_{\rm hh} + b_i S_{\rm hv} + c_i S_{\rm vv} + N_i', \quad i = 1{-}4 \qquad \text{(A1.1)}$$

where $\mathbf{M}' = (M_1',\ M_2',\ M_3',\ M_4')^T = [M_{\rm hh}', M_{\rm hv}', M_{\rm vh}', M_{\rm vv}']^T$ and $\mathbf{N}' = (N_1',\ N_2',\ N_3',\ N_4')^T$ are vectors corresponding to the LHS and the noise term on the RHS of (4), respectively, $\mathbf{S} = (S_{\rm hh}, S_{\rm hv}, S_{\rm vv})^T = (x, y, z)^T$, and the 4×1 coefficient vectors $\mathbf{a}$, $\mathbf{b}$, and $\mathbf{c}$ arise from the first term on the RHS of (4). This system can be resolved by assuming that the noise is independent identically distributed complex zero-mean Gaussian in all channels and by maximizing the likelihood. The log likelihood is proportional to

$$\begin{aligned} L &= \sum_1^4 |m_i - a_i x - b_i y - c_i z|^2 \\ &= \sum_1^4 (v_i - p_i x_1 + q_i x_2 - r_i y_1 + s_i y_2 - t_i z_1 + u_i z_2)^2 \\ &\quad + (w_i - p_i x_2 - q_i x_1 - r_i y_2 - s_i y_1 - t_i z_2 - u_i z_1)^2 \end{aligned}$$

where $m_i = v_i + jw_i$, $a_i = p_i + jq_i$, $b_i = r_i + js_i$, and $c_i = t_i + ju_i$.

Put

$$\begin{aligned} A = \frac{\partial L}{\partial x_1} &\propto \sum -p_i\,(v_i - p_i x_1 + q_i x_2 - r_i y_1 + s_i y_2 - t_i z_1 + u_i z_2) \\ &\quad - q_i (w_i - p_i x_2 - q_i x_1 - r_i y_2 - s_i y_1 - t_i z_2 - u_i z_1) \\ &= \sum -(p_i v_i + q_i w_i) + x_1 |a_i|^2 + y_1 (p_i r_i + q_i s_i) \\ &\quad + y_2 (-p_i s_i + q_i r_i) + z_1 (p_i t_i + q_i u_i) + z_2 (-p_i u_i + q_i t_i) \end{aligned}$$

$$\begin{aligned}B =& \frac{\partial L}{\partial x_2} \propto \sum q_i(v_i - p_i x_1 + q_i x_2 - r_i y_1 + s_i y_2 - t_i z_1 + u_i z_2) \\ & - p_i(w_i - p_i x_2 - q_i x_1 - r_i y_2 - s_i y_1 - t_i z_2 - u_i z_1) \\ =& \sum q_i v_i - p_i w_i + x_2|a_i|^2 + y_1(-q_i r_i + p_i s_i) \\ & + y_2(q_i s_i + p_i r_i) + z_1(-q_i t_i + p_i u_i) + z_2(q_i u_i + p_i t_i).\end{aligned}$$

Setting $A = B = 0$ and forming $A + jB$ yields

$$\sum -m_i a_i^* + x|a_i|^2 + y_1 b_i a_i^* + j y_2 b_i a_i^* + z_1 c_i a_i^* + j z_2 c_i a_i^* = 0$$

i.e.,

$$\sum_1^4 x|a_i|^2 + y b_i a_i^* + z c_i a_i^* = \sum_1^4 m_i a_i^*.$$

More compactly, writing $(\mathbf{a}, \mathbf{b}) = \sum_1^4 a_i b_i^*$, we have

$$x\,(\mathbf{a}, \mathbf{a}) + y(\mathbf{b}, \mathbf{a}) + z(\mathbf{c}, \mathbf{a}) = \ (\mathbf{m}, \mathbf{a}) \tag{A1.2a}$$

Similarly

$$x(\mathbf{a}, \mathbf{b}) + y(\mathbf{b}, \mathbf{b}) + z(\mathbf{c}, \mathbf{b}) = (\mathbf{m}, \mathbf{b}) \tag{A1.2b}$$

$$x(\mathbf{a}, \mathbf{c}) + y(\mathbf{b}, \mathbf{c}) + z(\mathbf{c}, \mathbf{c}) = (\mathbf{m}, \mathbf{c}). \tag{A1.2c}$$

This has the following form:

$$\mathbf{PS} = \mathbf{Q} \tag{A1.3}$$

where $\mathbf{P}$ is the coefficient vector in this system of equations, and $\mathbf{Q}$ is the RHS 3×1 vector; thus

$$\mathbf{S} = \mathbf{P}^{-1}\mathbf{Q}. \tag{A1.4}$$

Here, $\mathbf{P}^{-1}$ is a Hermitian matrix, i.e.,

$$\begin{aligned}&\mathbf{P}^{-1} \\ =& \frac{1}{\Delta}\begin{pmatrix} P_{22}P_{33} - |P_{23}|^2 & -P_{12}P_{33} + P_{13}P_{23}^* & P_{12}P_{23} - P_{13}P_{22} \\ -P_{12}^* P_{33} + P_{13}^* P_{23} & P_{11}P_{33} - |P_{13}|^2 & -P_{11}P_{23} + P_{13}P_{12}^* \\ P_{12}^* P_{23}^* - P_{13}^* P_{22} & -P_{11}P_{23}^* + P_{13}^* P_{12} & P_{11}P_{22} - |P_{12}|^2 \end{pmatrix}\end{aligned} \tag{A1.5a}$$

where

$$\begin{aligned}\Delta =& \det(\mathbf{P}) \\ =& P_{11}P_{22}P_{33} - \left(P_{11}|P_{23}|^2 + P_{22}|P_{13}|^2 + P_{33}|P_{12}|^2\right) \\ & + 2\mathrm{Re}(P_{12}P_{23}P_{13}^*).\end{aligned} \tag{A1.5b}$$

APPENDIX 2
NOISE STATISTICS AFTER CORRECTING FOR G

Using the first-order inverse of $\mathbf{G}$ given by (9), we can write the corrected noise terms in (7) as

$$\mathbf{N}' = \hat{\mathbf{G}}^{-1}\mathbf{N} = (N_1',\ N_2',\ N_3',\ N_4')^T.$$

Since

$$\hat{\mathbf{G}}^{-1} = \frac{1}{X}\begin{bmatrix} X & -\hat{\delta}_2 & -\hat{\delta}_4 & 0 \\ -\hat{\delta}_1 & X - \hat{\varepsilon}_1 & 0 & -\hat{\delta}_4 \\ -\hat{\delta}_3 & 0 & X - \hat{\varepsilon}_2 & -\hat{\delta}_2 \\ 0 & -\hat{\delta}_3 & -\hat{\delta}_1 & X - \hat{\varepsilon}_1 - \hat{\varepsilon}_2 \end{bmatrix}$$

where $X = 1 + 2\hat{\varepsilon}_1 + 2\hat{\varepsilon}_1$, the noise powers in the four channels of the corrected noise terms in (7) are then given by

$$V_N\,(1, 1 - 2\mathrm{Re}(\hat{\varepsilon}_1), 1 - 2\mathrm{Re}(\hat{\varepsilon}_2), 1 - 2\mathrm{Re}(\hat{\varepsilon}_1 + \hat{\varepsilon}_2))^T$$

where $V_N = \langle |N|^2 \rangle$ is the noise power in (1), which is assumed equal in all channels. Hence, the noise power is slightly changed after system correction. In addition, the noise channels become slightly correlated as follows:

$$\left\langle \hat{N}_1 \hat{N}_2^* \right\rangle \approx -V_N\left(\hat{\delta}_1^* X + \hat{\delta}_2 \frac{(X^* - \hat{\varepsilon}_1^*)}{|X|^2}\right) \approx -V_N\left(\hat{\delta}_1^* + \hat{\delta}_2\right)$$

$$\left\langle \hat{N}_1 \hat{N}_3^* \right\rangle \approx -V_N\left(\hat{\delta}_3^* X + \hat{\delta}_4 \frac{(X^* - \hat{\varepsilon}_2^*)}{|X|^2}\right) \approx -V_N\left(\hat{\delta}_3^* + \hat{\delta}_4\right)$$

$$\begin{aligned}\left\langle \hat{N}_4 \hat{N}_2^* \right\rangle &\approx -V_N \frac{\hat{\delta}_3(X^* - \hat{\varepsilon}_1^*) + \hat{\delta}_4^*(X - \hat{\varepsilon}_1 - \hat{\varepsilon}_2)}{|X|^2} \\ &\approx -V_N\left(\hat{\delta}_3 + \hat{\delta}_4^*\right)\end{aligned}$$

$$\begin{aligned}\left\langle \hat{N}_4 \hat{N}_3^* \right\rangle &\approx -V_N \frac{\hat{\delta}_1(X^* - \hat{\varepsilon}_2^*) + \hat{\delta}_2^*(X - \hat{\varepsilon}_1 - \hat{\varepsilon}_2)}{|X|^2} \\ &\approx -V_N\left(\hat{\delta}_1 + \hat{\delta}_2^*\right)\end{aligned}$$

$$\left\langle \hat{N}_1 \hat{N}_4^* \right\rangle \approx \left\langle \hat{N}_2 \hat{N}_3^* \right\rangle \approx 0.$$

Hence

$$\left\langle \hat{N}_1 \hat{N}_2^* \right\rangle \approx \left\langle \hat{N}_3 \hat{N}_4^* \right\rangle \qquad \left\langle \hat{N}_1 \hat{N}_3^* \right\rangle \approx \left\langle \hat{N}_2 \hat{N}_4^* \right\rangle.$$

Since the noise would remain Gaussian, the maximum likelihood analysis could be carried out with this more exact covariance matrix, but this has not been performed here.

APPENDIX 3
ERROR IN ESTIMATE OF σ_{hv}

Setting

$$\bar{\Sigma}_{13} = \frac{(\Delta\delta_1 + \Delta\delta_3)}{2}$$

$$\bar{\Sigma}_{24} = \frac{(\Delta\delta_2 + \Delta\delta_4)}{2}$$

$$\bar{\Sigma}_{\varepsilon} = \frac{(\Delta\varepsilon_1 + \Delta\varepsilon_2)}{2}$$

$$\bar{Y}_{21} = \frac{(\Delta\varepsilon_2 - \Delta\varepsilon_1)}{2}$$

(12) can be written as

$$\hat{S}_{\rm hv} = S_{\rm hh}(c^2\bar{\Sigma}_{13} - s^2\bar{\Sigma}_{24}) + S_{\rm vv}(c^2\bar{\Sigma}_{24} - s^2\bar{\Sigma}_{13}) + S_{\rm hv}(1+\bar{\Sigma}_\varepsilon) + cs(S_{\rm hh}+S_{\rm vv})\bar{Y}_{21} + (N'_{\rm hv}+N'_{\rm vh})/2 \tag{A3.1}$$

and then

$$\begin{aligned}|\hat{S}_{\rm hv}|^2 =& |S_{\rm hv}|^2|1+\bar{\Sigma}_\varepsilon|^2 + c^2s^2|S_{\rm hh}+S_{\rm vv}|^2|\bar{Y}_{21}|^2 \\ &+ |S_{\rm hh}|^2|c^2\bar{\Sigma}_{13} - s^2\bar{\Sigma}_{24}|^2 + |S_{\rm vv}|^2|c^2\bar{\Sigma}_{24} - s^2\bar{\Sigma}_{13}|^2 \\ &+ 2{\rm Re}\left\{S^*_{\rm hv}(1+\bar{\Sigma}^*_\varepsilon)\left[(c^2\bar{\Sigma}_{13} - s^2\bar{\Sigma}_{24})S_{\rm hh} + (c^2\bar{\Sigma}_{24} - s^2\bar{\Sigma}_{13})S_{\rm vv} + cs(S_{\rm hh}+S_{\rm vv})\bar{Y}_{21}\right]\right\} \\ &+ 2{\rm Re}\left\{(c^2\bar{\Sigma}_{13} - s^2\bar{\Sigma}_{24})(c^2\bar{\Sigma}^*_{24} - s^2\bar{\Sigma}^*_{13})S_{\rm hh}S^*_{\rm vv}\right\} \\ &+ 2cs{\rm Re}\left\{(c^2\bar{\Sigma}_{13} - s^2\bar{\Sigma}_{24})\left(|S_{\rm hh}|^2 + S_{\rm hh}S^*_{\rm vv}\right)\bar{Y}^*_{21} + (c^2\bar{\Sigma}_{24} - s^2\bar{\Sigma}_{13})\left(|S_{\rm vv}|^2 + S^*_{\rm hh}S_{\rm vv}\right)\bar{Y}^*_{21}\right\} \\ &+ \frac{|N'_{\rm hv}+N'_{\rm vh}|^2}{4} + \text{cross products with noise.}\end{aligned} \tag{A3.2}$$

Setting $\langle S_{\rm hh}S^*_{\rm vv}\rangle = Re^{j\theta}$ and averaging, assuming azimuthal symmetry, yields

$$\begin{aligned}\hat{\sigma}_{\rm hv} =& \sigma_{\rm hv}|1+\bar{\Sigma}_\varepsilon|^2 + c^2s^2(\sigma_{\rm hh}+\sigma_{\rm vv}+2R\cos\theta)|\bar{Y}_{21}|^2 \\ &+ \sigma_{\rm hh}|c^2\bar{\Sigma}_{13} - s^2\bar{\Sigma}_{24}|^2 + \sigma_{\rm vv}|c^2\bar{\Sigma}_{24} - s^2\bar{\Sigma}_{13}|^2 \\ &+ 2{\rm Re}\left\{(c^2\bar{\Sigma}_{13} - s^2\bar{\Sigma}_{24})(c^2\bar{\Sigma}^*_{24} - s^2\bar{\Sigma}^*_{13})Re^{j\theta}\right\} \\ &+ 2cs{\rm Re}\left\{(c^2\bar{\Sigma}_{13} - s^2\bar{\Sigma}_{24})(\sigma_{\rm hh}+Re^{j\theta})\bar{Y}^*_{21} + (c^2\bar{\Sigma}_{24} - s^2\bar{\Sigma}_{13})(\sigma_{\rm vv}+Re^{-j\theta})\bar{Y}^*_{21}\right\} \\ &+ \left(|N'_{\rm hv}|^2 + |N'_{\rm vh}|^2\right)/4.\end{aligned} \tag{A3.3}$$

If the channel imbalance is neglected and the noise powers in the HV and VH channels have the same value, i.e., σ'_n, then

$$\begin{aligned}\hat{\sigma}_{\rm hv} =& \sigma_{\rm hv} + \sigma_{\rm hh}\left|c^2\bar{\Sigma}_{13} - s^2\bar{\Sigma}_{24}\right|^2 + \sigma_{\rm vv}\left|c^2\bar{\Sigma}_{24} - s^2\bar{\Sigma}_{13}\right|^2 \\ &+ 2{\rm Re}\left\{(c^2\bar{\Sigma}_{13} - s^2\bar{\Sigma}_{24})(c^2\bar{\Sigma}^*_{24} - s^2\bar{\Sigma}^*_{13})Re^{j\theta}\right\} + \sigma'_n/2.\end{aligned} \tag{A3.4}$$

Set $\bar{\Sigma}_{13} = A_1e^{j\alpha_1}$, $\bar{\Sigma}_{24} = A_2e^{j\alpha_2}$, and $\varphi = \alpha_1 - \alpha_2$. Then

$$\begin{aligned}\hat{\sigma}_{\rm hv} - \sigma_{\rm hv} =& \sigma_{\rm hh}\left(c^4A_1^2 + s^4A_2^2 - 2c^2s^2A_1A_2\cos\varphi\right) + \sigma_{\rm vv}\left(c^4A_2^2 + s^4A_1^2 - 2c^2s^2A_1A_2\cos\varphi\right) \\ &+ 2R{\rm Re}\left\{\left(c^4\bar{\Sigma}_{13}\bar{\Sigma}^*_{24} + s^4\bar{\Sigma}^*_{13}\bar{\Sigma}_{24} - s^2c^2\left(A_1^2+A_2^2\right)\right)e^{j\theta}\right\} + \sigma'_n/2\end{aligned}$$

i.e.,

$$\begin{aligned}\hat{\sigma}_{\rm hv} - \sigma_{\rm hv} =& \sigma_{\rm hh}\left(c^4A_1^2 + s^4A_2^2 - 2c^2s^2A_1A_2\cos\varphi\right) + \sigma_{\rm vv}\left(c^4A_2^2 + s^4A_1^2 - 2c^2s^2A_1A_2\cos\varphi\right) \\ &+ 2RA_1A_2\left(c^4\cos(\theta+\varphi) + s^4\cos(\theta-\varphi)\right) - 2Rs^2c^2\left(A_1^2+A_2^2\right)\cos\theta + \sigma'_n/2.\end{aligned} \tag{A3.5}$$

Setting $E = \hat{\sigma}_{\rm hv} - \sigma_{\rm hv}$, we have

$$\begin{aligned}\frac{\partial E}{\partial\,\Omega} =& 2\sin 2\Omega\left(\sigma_{\rm hh}\left(-c^2A_1^2 + s^2A_2^2 - A_1A_2\cos\varphi\cos 2\Omega\right) + \sigma_{\rm vv}\left(-c^2A_2^2 + s^2A_1^2 - A_1A_2\cos\varphi\cos 2\Omega\right)\right. \\ &+ 2RA_1A_2\left(-c^2\cos(\theta+\varphi) + s^2\cos(\theta-\varphi)\right) \\ &\left. - R(A_1^2+A_2^2)\cos\theta\cos 2\Omega\right).\end{aligned} \tag{A3.6}$$

Hence, there are extrema when $\sin 2\Omega = 0$, i.e., $\Omega = n\pi/2$; thus, $s^2 = 1$ and $c^2 = 0$, or $s^2 = 0$ and $c^2 = 1$.

If $s^2 = 1$, then $\Omega = k\pi + \pi/2$, and

$$E = \sigma_{\rm hh}A_2^2 + \sigma_{\rm vv}A_1^2 + 2RA_1A_2\cos(\theta-\varphi) + \sigma'_n/2. \tag{A3.7a}$$

However, if $c^2 = 1$, then $\Omega = k\pi$, and

$$E = \sigma_{\rm hh}A_1^2 + \sigma_{\rm vv}A_2^2 + 2RA_1A_2\cos(\theta+\varphi) + \sigma'_n/2. \tag{A3.7b}$$

Clearly, both errors are maximized if the cosine term takes a value of 1 and increase as either A_1 or A_2 increases. Hence, if both A_1 and A_2 have the same absolute maximum, i.e., A_M, then the maximum error is

$$A_M^2(\sigma_{\rm hh} + \sigma_{\rm vv} + 2R) + \sigma'_n/2.$$

Since $A_1 = |\Delta\delta_1 + \Delta\delta_3|/2$ and $A_2 = |\Delta\delta_2 + \Delta\delta_4|/2$, then, for given amplitudes of $\Delta\delta_i$, A_i will be maximized if $\arg\Delta\delta_1 = \arg\Delta\delta_3$, which implies that $\arg\Delta\delta_1 = \arg\bar{\Sigma}_{13} = \alpha_1$ and that $\arg\Delta\delta_2 = \arg\Delta\delta_4 = \arg\bar{\Sigma}_{24} = \alpha_2$.

If all the $\Delta\delta_i$ have the same largest permitted amplitude $\Delta\delta_M$, then $\Delta\delta_1 = \Delta\delta_3$, $\Delta\delta_2 = \Delta\delta_4$, and $|\Delta\delta_i| = \Delta\delta_M$ for all i, and $A_M = \Delta\delta_M$. Furthermore, condition $\cos(\theta-\varphi) = 1$ means that the maximum of (A3.7a) occurs if $\theta - \varphi = 2k\pi$; thus, $\alpha_1 = \alpha_2 + \theta + 2k\pi$, and $\Delta\delta_1 = e^{j\theta}\Delta\delta_2$. Similarly, the maximum of (A3.7b) occurs if $\theta + \varphi = 2k\pi$ so that $\alpha_1 = \alpha_2 - \theta + 2k\pi$ and $\Delta\delta_1 = e^{-j\theta}\Delta\delta_2$.

In both cases, the maximum possible error is

$$\hat{\sigma}_{\rm hv} - \sigma_{\rm hv} = \Delta\delta_M^2(\sigma_{\rm hh} + \sigma_{\rm vv} + 2R) + \sigma_n/2 \tag{A3.8}$$

where, using Appendix 2, σ'_n has been approximated by σ_n, i.e., the NESZ in the original measurements (1).

APPENDIX 4
ERROR IN ESTIMATES OF COPOLARIZED CHANNELS

From (6), we have

$$\begin{aligned}\hat{S}_{\rm hh} =& S_{\rm hh}(\hat{c}^2c^2 + 2\hat{c}\hat{s}cs + \hat{s}^2s^2)\\ &+ S_{\rm vv}(-\hat{c}^2s^2 + 2\hat{c}\hat{s}cs - \hat{s}^2c^2)\\ &+ \hat{c}^2\left(S_{\rm hv}\Sigma_{24} - X_{24}cs(S_{\rm hh} + S_{\rm vv})\right)\\ &- \hat{s}^2\left(S_{\rm hv}\Sigma_{31} - X_{31}cs(S_{\rm hh} + S_{\rm vv})\right)\\ &+ \hat{c}\hat{s}\left(X_{31}(c^2S_{\rm hh} - s^2S_{\rm vv})\right.\\ &\qquad \left.+X_{24}(-s^2S_{\rm hh} + c^2S_{\rm vv})\right)\\ &+ \hat{c}\hat{s}\left(S_{\rm hv}Y_{21} + \Sigma_\varepsilon cs\left(S_{\rm hh} + S_{\rm vv}\right)\right)\\ &- \hat{s}^2\Sigma_\varepsilon(-s^2S_{\rm hh} + c^2S_{\rm vv})\\ &+ \hat{c}^2N'_{\rm hh} + \hat{c}\hat{s}\left(N'_{\rm vh} - N'_{\rm hv}\right) - \hat{s}^2N'_{\rm vv}\end{aligned} \tag{A4.1}$$

where $\Sigma_{24} = \Delta\delta_2 + \Delta\delta_4$, $\Sigma_{31} = \Delta\delta_3 + \Delta\delta_1$, $X_{24} = \Delta\delta_2 - \Delta\delta_4$, $X_{31} = \Delta\delta_3 - \Delta\delta_1$, $\Sigma_\varepsilon = \Delta\varepsilon_1 + \Delta\varepsilon_2$, and $Y_{21} = \Delta\varepsilon_2 - \Delta\varepsilon_1$.

Setting $C = \cos(2\Omega)$ and $S = \sin(2\Omega)$, with $\hat{C}$ and $\hat{S}$ being their estimated values, this can be written as

$$\begin{aligned}\hat{S}_{\rm hh} =& \frac{S_{\rm hh}}{2}(\hat{C}C + S\hat{S} + 1) + \frac{S_{\rm vv}}{2}(\hat{C}C + S\hat{S} - 1)\\ &+ \frac{S_{\rm hh}}{4}\left\{X_{31}\left(S(1-\hat{C}) + \hat{S}(1+C)\right)\right.\\ &\qquad \left.-X_{24}\left(S(1+\hat{C}) + \hat{S}(1-C)\right)\right\}\\ &+ \frac{S_{\rm vv}}{4}\left\{X_{31}\left(S(1-\hat{C}) - \hat{S}(1-C)\right)\right.\\ &\qquad \left.+X_{24}\left(\hat{S}(1+C) - S(1+\hat{C})\right)\right\}\\ &+ \frac{S_{\rm hv}}{2}\left((1+\hat{C})\Sigma_{24} - (1-\hat{C})\Sigma_{31}\right)\\ &+ \frac{\Sigma_\varepsilon}{4}\left(S_{\rm hh}\left(S\hat{S} + (1-C)(1-\hat{C})\right)\right.\\ &\qquad \left.+S_{\rm vv}\left(S\hat{S} - (1+C)(1-\hat{C})\right)\right)\\ &+ \frac{S_{\rm hv}}{2}\hat{S}Y_{21}\\ &+ \frac{1}{2}\left\{(1+\hat{C})N'_{\rm hh} + \hat{S}\left(N'_{\rm vh} - N'_{\rm hv}\right) - (1-\hat{C})N'_{\rm vv}\right\}.\end{aligned} \tag{A4.2}$$

Putting $\hat{\Omega} = \Omega + \omega/2$, for a small error in Ω, we can make the approximations as follows:

$$\hat{C} = \cos(2\Omega + \omega) \approx C - \omega S$$
$$\hat{S} = \sin(2\Omega + \omega) \approx S + \omega C$$

and (A4.2) becomes

$$\begin{aligned}\hat{S}_{\rm hh} \approx& S_{\rm hh}\\ &+ \frac{S_{\rm hh}}{4}(X_{31}\left[2S + \omega(1+C)\right] - X_{24}\left[2S - \omega(1-C)\right])\\ &+ \omega\frac{S_{\rm vv}}{4}\left(X_{31}(1-C) + X_{24}(1+C)\right)\\ &+ \frac{S_{\rm hv}}{2}\left((1+C-\omega S)\Sigma_{24} - (1-C+\omega S)\Sigma_{31}\right)\\ &+ \frac{\Sigma_\varepsilon}{4}\left(S_{\rm hh}(2-2C+\omega S) - \omega SS_{\rm vv}\right)\\ &+ \frac{S_{\rm hv}}{2}(S + \omega C)Y_{21}\\ &+ \frac{1}{2}\left\{(1+\hat{C})N'_{\rm hh} + \hat{S}\left(N'_{\rm vh} - N'_{\rm hv}\right) - (1-\hat{C})N'_{\rm vv}\right\}.\end{aligned} \tag{A4.3}$$

If we neglect the terms involving second-order products of small quantities (such as ωX_{31}), then (A4.3) reduces to

$$\begin{aligned}\hat{S}_{\rm hh} \approx& S_{\rm hh} + \frac{S_{\rm hh}}{2}S\left(X_{31} - X_{24}\right)\\ &+ \frac{S_{\rm hv}}{2}\left((1+C)\Sigma_{24} - (1-C)\Sigma_{31}\right)\\ &+ S_{\rm hh}(1-C)\frac{\Sigma_\varepsilon}{2} + \frac{S_{\rm hv}}{2}SY_{21}\\ &+ \frac{1}{2}\left\{(1+\hat{C})N'_{\rm hh} + \hat{S}\left(N'_{\rm vh} - N'_{\rm hv}\right) - (1-\hat{C})N'_{\rm vv}\right\}.\end{aligned} \tag{A4.4}$$

Hence

$$\begin{aligned}\hat{\sigma}_{\rm hh} \approx& \sigma_{\rm hh}\left\{1 + {\rm Re}\left(S(X_{31} - X_{24}) + (1-C)\Sigma_\varepsilon\right)\right\}\\ &+ {\rm Re}\left\{S^*_{\rm hh}S_{\rm hv}\left((1+C)\Sigma_{24} - (1-C)\Sigma_{31} + SY_{21}\right)\right\}\\ &+ \frac{1}{4}\left\{(1+\hat{C})^2\left|N'_{\rm hh}\right|^2 + \hat{S}^2\left(\left|N'_{\rm vh}\right|^2 + \left|N'_{\rm hv}\right|^2\right)\right.\\ &\qquad \left.+(1-\hat{C})^2\left|N'_{\rm vv}\right|^2\right\}\end{aligned} \tag{A4.5}$$

where we again have neglected the terms involving second-order products of small quantities and assumed that the noise is uncorrelated with the signal and between channels. Note that, if the noise powers all have the same value, i.e., σ'_n, then the total contribution from the noise is σ'_n.

The corresponding expressions for VV are

$$\begin{aligned}\hat{S}_{\rm vv} \approx& S_{\rm vv} + \frac{S_{\rm vv}}{2}S(-X_{31} + X_{24})\\ &+ \frac{S_{\rm hv}}{2}\left((1+C)\Sigma_{31} - (1-C)\Sigma_{24}\right)\\ &+ S_{\rm vv}(1+C)\frac{\Sigma_\varepsilon}{2} + \frac{S_{\rm hv}}{2}SY_{21}\\ &+ \frac{1}{2}\left\{-(1-\hat{C})N'_{\rm hh} + \hat{S}\left(N'_{\rm vh} - N'_{\rm hv}\right) + (1+\hat{C})N'_{\rm vv}\right\}\end{aligned} \tag{A4.6}$$

$$\begin{aligned}\hat{\sigma}_{\rm vv} \approx& \sigma_{\rm vv}\left\{1 + {\rm Re}\left(S(-X_{31} + X_{24}) + (1+C)\Sigma_\varepsilon\right)\right\}\\ &+ {\rm Re}\left\{S^*_{\rm vv}S_{\rm hv}\left((1+C)\Sigma_{31} - (1-C)\Sigma_{24} + SY_{21}\right)\right\}\\ &+ \frac{1}{4}\left\{(1-\hat{C})^2\left|N'_{\rm hh}\right|^2 + \hat{S}^2\left(\left|N'_{\rm vh}\right|^2 + \left|N'_{\rm hv}\right|^2\right)\right.\\ &\qquad \left.+(1+\hat{C})^2\left|N'_{\rm vv}\right|^2\right\}.\end{aligned} \tag{A4.7}$$

ACKNOWLEDGMENT

The authors would like to thank the reviewers for their helpful questions and comments that led to a much improved paper.

REFERENCES

[1] A. Freeman, "Calibration of linearly polarized polarimetric SAR data subject to Faraday rotation," *IEEE Trans. Geosci. Remote Sens.*, vol. 42, no. 8, pp. 1617–1624, Aug. 2004.

[2] A. Freeman, X. Pi, and B. Chapman, "Calibration of PALSAR polarimetric data," presented at the 4th Int. Workshop Science Applications SAR Polarimetric Interferometry—*PolInSAR*, Frascati, Italy, Jan. 26–30, 2009, Paper ESA SP-668, Apr. 2009.

[3] A. Takeshiro, T. Furuya, and H. Fukuchi, "Verification of polarimetric calibration method including Faraday rotation compensation using PALSAR data," *IEEE Trans. Geosci. Remote Sens.*, vol. 47, no. 12, pp. 3960–3968, Dec. 2009.

[4] J. Chen, S. Quegan, and X. J. Yin, "Calibration of spaceborne linearly polarized low frequency SAR using polarimetric selective radar calibrators," *Progr. Electromagn. Res.*, vol. 114, pp. 89–111, 2011.

[5] J. Chen and S. Quegan, "Improved estimators of Faraday rotation in spaceborne polarimetric SAR data," *IEEE Geosci. Remote Sens. Lett.*, vol. 7, no. 4, pp. 846–850, Oct. 2010.

[6] N. C. Rogers and S. Quegan, "The accuracy of Faraday rotation estimation in satellite synthetic aperture radar images," *IEEE Trans. Geosci. Remote Sens.*, vol. 52, no. 8, pp. 4799–4807, Aug. 2014.

[7] S. Quegan *et al.*, Report for mission selection: Biomass, Eur. Space Agency, Noordwijk, The Netherlands, ESA SP 1324/1 (vol. 3), 2012.

[8] T. Le Toan *et al.*, "The BIOMASS Mission: Mapping global forest biomass to better understand the terrestrial carbon cycle," *Remote Sens. Environ.*, vol. 115, no. 11, pp. 2850–2860, Nov. 2011.

[9] S. Quegan and M. R. Lomas, "The impact of system effects on estimates of Faraday rotation from synthetic aperture radar measurements," *IEEE Trans. Geosci. Remote Sens.*, vol. 53, no. 8, pp. 4284–4298, Aug. 2015.

[10] A. Freeman, "SAR calibration: An overview," *IEEE Trans. Geosci. Remote Sens.*, vol. 30, no. 6, pp. 1107–1121, Nov. 1992.

[11] S. Quegan, "A unified algorithm for phase and crosstalk calibration of polarimetric data—Theory and observations," *IEEE Trans. Geosci. Remote Sens.*, vol. 32, no. 1, pp. 89–99, Jan. 1994.

[12] S. H. Bickel and R. H. T. Bates, "Effects of magneto-ionic propagation on the polarization scattering matrix," *Proc. IRE*, vol. 53, no. 8, pp. 1089–1091, Aug. 1965.

[13] R.-Y. Qi and Y.-Q. Jin, "Analysis of the effects of Faraday rotation on spaceborne polarimetric SAR observations at P-band," *IEEE Trans. Geosci. Remote Sens.*, vol. 45, no. 5, pp. 1115–1122, May 2007.

[14] F. J. Meyer and J. B. Nicoll, "Prediction, detection, and correction of Faraday rotation in full-polarimetric L-band SAR data," *IEEE Trans. Geosci. Remote Sens.*, vol. 46, no. 10, pp. 3076–3086, Oct. 2008.

[15] A. Beaudoin *et al.*, "Retrieval of forest biomass from SAR data," *Int. J. Remote Sens.*, vol. 15, no. 14, pp. 2777–2796, Sep. 1994.

[16] M. C. Dobson *et al.*, "Dependence of radar backscatter on coniferous forest biomass," *IEEE Trans. Geosci. Remote Sens.*, vol. 30, no. 2, pp. 412–415, Mar. 1992.

[17] D. H. Hoekmanand and M. J. Quinones, "Land cover type and biomass classification using AirSAR data for evaluation of monitoring scenarios in the Colombian Amazon," *IEEE Trans. Geosci. Remote Sens.*, vol. 38, no. 2, pp. 685–696, Mar. 2000.

[18] T. Le Toan, A. Beaudoin, J. Riom, and D. Guyon, "Relating forest biomass to SAR data," *IEEE Trans. Geosci. Remote Sens.*, vol. 30, no. 2, pp. 403–411, Mar. 1992.

[19] E. J. Rignot, R. Zimmerman, and J. J. van Zyl, "Spaceborne applications of P-band imaging radar for measuring forest biomass," *IEEE Trans. Geosci. Remote Sens.*, vol. 33, no. 5, pp. 1162–1169, Sep. 1995.

[20] G. Sandberg, L. M. H. Ulander, J. E. S. Fransson, J. Holmgren, and T. Le Toan, "L- and P-band backscatter intensity for biomass retrieval in hemiboreal forest," *Remote Sens. Environ.*, vol. 115, no. 11, pp. 2874–2886, Nov. 2011.

[21] M. J. Soja, G. Sandberg, and L. M. H. Ulander, "Regression-based retrieval of boreal forest biomass in sloping terrain using P-band SAR backscatter intensity data," *IEEE Trans. Geosci. Remote Sens.*, vol. 51, no. 5, 2646–2665, May 2013.

[22] G. Sandberg, L. M. H. Ulander, J. Wallerman, and J. E. S. Fransson, "Measurements of forest biomass change using P-band synthetic aperture radar backscatter," *IEEE Trans. Geosci. Remote Sens.*, vol. 52, no. 10, pp. 6047–6061, Oct. 2014.

[23] M. Fujita, "Polarimetric calibration of space SAR data subject to Faraday rotation—A three target approach," in *Proc. IEEE IGARSS*, Seoul, Korea, 2005, pp. 5497–5500.

[24] H. Kimura, "Calibration of polarimetric PALSAR imagery affected by Faraday rotation using polarization orientation," *IEEE Trans. Geosci. Remote Sens.*, vol. 47, no. 12, pp. 3943–3950, Dec. 2009.

[25] M. Shimada, O. Isoguchi, T. Tadono, and K. Isono, "PALSAR radiometric and geometric calibration," *IEEE Trans. Geosci. Remote Sens.*, vol. 47, no. 12, pp. 3915–3932, Dec. 2009.

[26] R. Touzi and M. Shimada, "Polarimetric PALSAR calibration," *IEEE Trans. Geosci. Remote Sens.*, vol. 47, no. 12, pp. 3951–3959, Dec. 2009.

[27] M. Shimada, "Model-based polarimetric SAR calibration method using forest and surface-scattering targets," *IEEE Trans. Geosci. Remote Sens.*, vol. 49, no. 5, 1712–1733, May 2011.

[28] P. Wright, S. Quegan, N. Wheadon, and D. Hall, "Faraday rotation effects on L-band spaceborne SAR data," *IEEE Trans. Geosci. Remote Sens.*, vol. 41, no. 12, 2735–2744, Dec. 2003.

[29] P. López-Dekker *et al.*, "BIOMASS End-to-End mission performance simulator," in *Proc. IEEE IGARSS*, Vancouver, BC, Canada, 2011, pp. 4249–4252.

[30] J.-S. Lee, D. L. Schuler, and T. L. Ainsworth, "Polarimetric SAR data compensation for terrain azimuth slope variation," *IEEE Trans. Geosci. Remote Sens.*, vol. 38, no. 5, 2153–2163, Sep. 2000.

Shaun Quegan (M'90) received the B.A. and M.Sc. degrees in mathematics from the University of Warwick, Coventry, U.K., in 1970 and 1972, respectively, and the Ph.D. degree from the University of Sheffield, Sheffield, U.K., in 1982.

From 1982 to 1986, he was a Research Scientist with the Marconi Research Centre, Great Baddow, U.K., where he led the Remote Sensing Applications Group from 1984 to 1986. In 1986, he established the SAR Research Group at the University of Sheffield, where he became a Professor in 1993. In the same year, he helped inaugurate the Sheffield Centre for Earth Observation Science, University of Sheffield. In 2001, he became the Director of the U.K. National Environmental Research Council Centre for Terrestrial Carbon Dynamics. This multiinstitutional center was concerned with assimilating Earth observation (EO) and other data into the process models of the land component of the carbon cycle and now forms part of the U.K. National Centre for Earth Observation. His broad interests in the physics, systems, and data analysis aspects of radar remote sensing are now subsumed in the more general aim of exploiting many sorts of EO technology to give greater quantitative understanding of the carbon cycle.

Mark R. Lomas received the B.Sc. and Ph.D. degrees in applied and computational mathematics from the University of Sheffield, Sheffield, U.K., in 1989 and 1995, respectively. His Ph.D. studies investigated the phenomenon of voltage collapse.

Since 1994, he has been a Research Associate with the Department of Animal and Plant Science and the School of Mathematics and Statistics, University of Sheffield, where he mainly works on the global land surface carbon and hydrological cycles via dynamic vegetation models, specifically the Sheffield Dynamic Global Vegetation Model and its predecessor, the Dynamic Global Phytogeography (DOLY) model, which he played a key role in developing. A large part of his research has been concerned with utilizing Earth observation data to test and improve these models.

Dr. Lomas' Ph.D. studies were funded by the National Grid.